UCRL 10187

University of California

Ernest O. Lawrence Radiation Laboratory

NEUTRAL PIONS FROM PROTON-PROTON COLLISIONS AT 735 MeV

Berkeley, California

DISCLAIMER

Research and Development

UCRL-10187
UC-34 Physics
TID-4500 (17th Ed.)

1,2,3
63

UNIVERSITY OF CALIFORNIA

Lawrence Radiation Laboratory
Berkeley, California

Contract No. W-7405-eng-48

NEUTRAL PIONS FROM PROTON-PROTON COLLISIONS AT 735 MeV

Gilbert D. Mead

(Ph. D. Thesis)

May 8, 1962

Printed in USA. Price $2.00. Available from the
Office of Technical Services
U. S. Department of Commerce
Washington 25, D.C.

NEUTRAL PIONS FROM PROTON-PROTON COLLISIONS AT 735 MeV

Contents

Abstract v

I. Introduction 1

A. Review of Pion Production in Nucleon-Nucleon Collisions . . 1

B. The Reaction $p + p \rightarrow p + p + \pi^0$ 4

C. Motivation for this Experiment 7

II. Experimental Method 11

A. Introduction 11

B. Physical Layout 12

1. Cave Layout 12

2. Proton Beam 12

3. Hydrogen Target 18

C. Physical Apparatus 20

1. Spectrometers 20

2. Anticoincidence Counter 27

D. Electronic Apparatus 30

E. Experimental Procedures 32

III. Method of Analysis 33

A. General Method 33

B. Description of the Data Analysis Program 34

C. Normalizing Procedures 36

IV. Results 38

A. Laboratory Gamma-Ray Spectra 38

B. C. M. Gamma-Ray and Pion Spectra and Total Cross Section . 40

1. Gamma-Ray Spectra 40

2. Method used to get Pion Distributions 40

3. Resulting Pion Distributions 45

4. Total Cross Section 47

V. Summary and Conclusions 49

Appendices 52

A. Theory of the Pair Spectrometer 52

B. Resolving Power of the Spectrometer 57

1. Geometric Resolving Power 57
2. Radiation Straggling 58
3. Other Factors 61
C. Spectrometer Parameters 64
D. Vertical Scattering Correction 66
E. Pair-Production Cross-Section Formulae 70
F. The Kinematics of π^0 Decay 72
1. Determination of Gamma-Ray Spectra from π^0 Distributions 73
2. Transformation of Gamma-Ray Spectra 76
3. Determination of Total Cross Sections 78
Acknowledgments 80
References 81

NEUTRAL PIONS FROM PROTON-PROTON COLLISIONS AT 735 MeV

Gilbert D. Mead

Lawrence Radiation Laboratory
University of California
Berkeley, California

May 8, 1962

ABSTRACT

An investigation has been made of the reaction $p + p \rightarrow p + p + \pi^0$ at an incident proton energy of 735 MeV. The external proton beam of the 184-inch synchrocyclotron bombarded a liquid hydrogen target. Gamma-ray spectra were measured at lab angles of 6, 32, and 60 deg with respect to the proton beam. Two high-resolution pair spectrometers were used to analyze the photons. Computer codes were used to make all necessary corrections to the data and determine the final spectra.

No evidence is found for gamma rays produced from any source other than π^0 decay. The cross section for π^0 production was measured to be 3.46±0.25 mb. Using a least-squares analysis, angular and momentum distributions for the neutral pion in the two-proton c.m. system were determined from the photon spectra. The pion angular distribution is given by

$$\frac{d\sigma_{\pi^0}}{d\Omega} = \frac{\sigma_{tot}}{4\pi} \left[0.834 + 0.099 \left(3 \cos^2\theta\right) + 0.067 \left(5 \cos^4\theta\right) \right] .$$

That is, 83% of the pions are produced with isotropic distribution. This result is consistent with the isobar model of pion production. Pion momentum distributions are given for several c.m. angles. These also support the isobar model.

I. INTRODUCTION

A. Review of Pion Production in Nucleon-Nucleon Collisions

Since the discovery of the pi meson, a large amount of effort, both theoretical and experimental, has been spent trying to understand the basic mechanisms involved in pion production in nucleon-nucleon collisions. There is still no comprehensive theory able to make detailed, precise calculations and predictions. Several theories have been presented, however, which provide qualitative and semiquantitative understanding of the pion production process in various energy regions.

Perhaps our clearest understanding is in the region near threshold. The first experiments were performed using cyclotrons whose proton energies were only slightly above threshold for pion production. This early work, along with a phenomenological theory that provides a good understanding of the experimental results, is summarized in review articles by Rosenfeld[1] and Gell-Mann and Watson.[2]

At high energies, the arguments that apply near threshold become less applicable. Final-state interactions between the emergent pion and one of the nucleons must be considered. The isobar model, as developed by Lindenbaum and Sternheimer,[3] assumes that pion production proceeds via the intermediate formation of a nucleon isobar, which subsequently decays into a nucleon and a pion:

$$N + N \rightarrow N + N^{*}$$
$$N^{*} \rightarrow N + \pi \quad .$$

This nucleon isobar is assumed to be in the isotopic spin $T = 3/2$, angular momentum $J = 3/2$ resonant state. Its mass corresponds to the total energy of the pion-nucleon system at the $3/2 - 3/2$ scattering resonance. Since the π-N resonance has a finite width, the mass of the isobar will not be unique, but has a distribution centered on the value of 1.23 BeV. This theory assumes that the isobar exists long enough to allow it to separate from the other nucleon before decaying. Thus final-state interactions between the decay products of the isobar and the other nucleon are small.

If sufficient energy is available, double-pion production can proceed via the excitation and decay of both nucleons. One can also excite higher isobaric levels corresponding to the higher resonances in the π-N system.[4]

This theory has been quite successful in explaining the experimental results of pion production at cosmotron energies (0.8 - 3.0 BeV), but its predictions are quite different from those of the Fermi statistical model.[5] Fermi assumed that thermodynamic equilibrium was established inside a collision volume of radius equal to the pion Compton wave length. The relative probability of a final state was simply proportional to the phase space available for this state. Thus it was assumed that matrix elements for all final states were essentially the same. Although the predictions were useful at high cosmic-ray energies (10 to 100 BeV), at energies of 1 to 3 BeV its predictions of pion multiplicities and pion spectra differed significantly from the experimental results. It thus appears that the pion-nucleon final-state interactions play a major role at these energies.

Mandelstam has developed a resonant theory to apply in the intermediate energy region (up to about 700 MeV).[6] Just as with the phenomenological description at threshold energies, the pion-production process is analyzed in terms of a limited number of angular-momentum final states. The difference is that whereas Gell-Mann and Watson consider states wherein the pion is in an S- or P-state with respect to the whole nucleon-nucleon system, Mandelstam assumes that the pion is in a 3/2 - 3/2 resonance state with one nucleon, and the second nucleon is in an S- or P-state with respect to this resonant system. He develops a theory with adjustable parameters for six basic types of transitions. By somewhat arbitrarily setting some of them equal to each other, he is left with three parameters that can be fixed from the experimental values of three basic cross sections. The resulting theory agrees quite adequately with most of the experimental results in the energy region to which it has been applied. Some modification is necessary, however, in the threshold region.

These theories all have one basic inadequacy: they are all essentially phenomenological in nature. That is, they fail to provide any underlying mechanism for the production of the resonant state. They all depend upon experimental data to provide numerical values for the necessary parameters; no absolute cross sections are predicted. In order to go further, one must assume a specific mechanism associated with some Feynman diagram, so that field theoretical calculations can be made.

Recently several authors have suggested theories wherein such a mechanism is provided.[7-9] This mechanism consists of the exchange of a single virtual pion, for which a Feynman diagram is as follows:

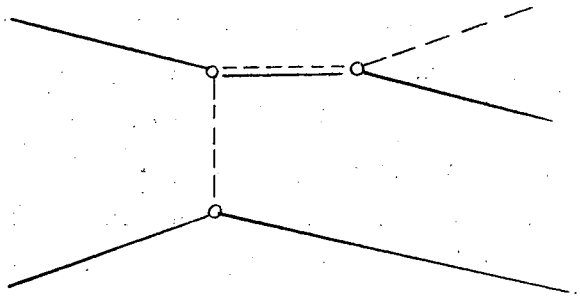

Here solid lines are nucleons and dotted lines are pions. In this example we show the production of an isobar by the exchange of a single virtual pion. The isobar then decays to produce the pion. This mechanism has been called the peripheral interaction model or the long-range interaction model, so called because the interaction between nucleons seems to take place in the pion cloud rather than at the much smaller absorptive core. Bonsignori and Selleri have used this theory to calculate energy distributions and cross sections for incident proton energies of 970 MeV.[7] This energy corresponds to that used by Batson et al. at Birmingham to produce inelastic proton-proton interactions in a hydrogen-filled diffusion cloud chamber.[10] The peripheral interaction model predicts results which are well verified by this experiment. On the other hand, predictions of the statistical model differ significantly from the experimental results.

The peripheral interaction model has been applied mainly in the region of $\geq$ 1-BeV incident nucleon energy. This is primarily because at lower energies only a few angular momentum states are important, and threshold effects are still dominant. Single-pion exchange is only one of many fundamental processes that can contribute to the pion-production matrix element at low energies.

B. The Reaction $p + p \rightarrow p + p + \pi^0$

The reaction $p + p \rightarrow p + p + \pi^0$ has been of particular interest for several reasons. First of all, in the notation of Rosenfeld,[1] the cross section is pure σ_{11}; that is, the isotopic spin of the nucleons equals 1 in both the initial and final states. Most other reactions in which pions are produced involve combinations of the three basic cross sections σ_{11}, σ_{10}, and σ_{01}. For instance, the reaction $p + p \rightarrow p + n + \pi^+$ is a sum of σ_{11} and σ_{10}.

A second reason for the interest in the $p + p \rightarrow \pi^0$ reaction is its rather unusual behavior near threshold. The cross section is extremely low as compared with positive pion production, and rises rapidly as the incident proton energy increases. This is because the state which is most important in π^+ production near threshold (Class Sp in Rosenfeld's notation) is not available to the σ_{11} cross section. When the Pauli principle is applied, one cannot conserve angular momentum and parity simultaneously.

Studies of neutral pion production, however, are difficult to perform. This is true for a number of reasons. The pion itself can never be observed, due to its neutral charge and extremely short lifetime. Analysis of the gamma rays into which it normally decays is also not easy. An instrument with high efficiency cannot measure gamma-ray energies with any precision. On the other hand, a high-resolution instrument such as the pair spectrometer which we use has inherently low efficiency. It is very difficult to detect the two gamma rays simultaneously, and even more difficult to also measure the energy of either one or both. A hydrogen bubble chamber is very inefficient for detecting gamma rays because of the low cross section for pair production. If a heavier element is used as the liquid for a bubble chamber, the event can no longer be simply analyzed in terms of fundamental particle interactions.

Most of the experiments which have been done are of three types: those that simply detect and count gamma rays at various laboratory angles, those that measure the energy spectrum of the gamma rays, and those that analyze one or both of the recoil nucleons.

We now summarize the main results of the experiments on neutral pion production, especially in proton-proton collisions, since 1950.

Soon after discovery of the neutral pion[11,12] it was noted by Hales et al.[13] that the gamma-ray yield from protons on complex nuclei depended only on the number of neutrons in the nucleus and was essentially independent

of the number of protons. Actual cross-section measurements for $p + p \rightarrow p + p + \pi^0$ by Mather and Martinelli,[14] Moyer and Squire,[15] Marshall et al.,[16] Stallwood et al.,[17] and York et al.,[18] at energies from 340 through 447 MeV confirmed both the low cross section near threshold (10 μb at 340 MeV[14,19] as compared with 150 μb for π^0 production on neutrons) and the steep excitation function. Further cross-section measurements have been made up to 670 MeV by Tiapkin et al.,[20] Soroko,[21] Prokoshkin and Tiapkin,[22] and Dunaitsev and Prokoshkin.[23] The result of these measurements, along with a value in nuclear emulsion at 925 MeV,[24] and a value obtained from a hydrogen diffusion cloud chamber at 970 MeV,[10] are plotted in Fig. 1. The value of 3.46±0.25 mb obtained by us at 735 MeV is also shown. These are all plotted as a function of η_{max}, the maximum pion momentum in the center-of-mass system, in units of $m_{\pi^0}c$. It is seen that the cross section continues to rise rapidly up to around 600 MeV, after which it begins to level off to a value of around 4 mb. This general behavior is in good agreement with Mandelstam's resonance theory, when modified at energies below 500 MeV for nonresonant Ss transitions. Mandelstam's theory predicts a peak in the cross section at about 800 MeV.

The information on angular distributions is much more limited, primarily becuase the gamma-ray angular distributions only weakly reflect the neutral-pion angular distributions. One must measure gamma fluxes very accurately to obtain even limited accuracy for pion distributions, unless one can measure the gamma energy spectra as well.

The c.m. angular distributions can be expressed by expanding the distributions in the even powers of $\cos\theta_{c.m.}$, i.e.,

$$\frac{d\sigma}{d\Omega} \propto 1 + 3b\cos^2\theta + 5c\cos^4\theta + \cdots .$$

Odd powers of $\cos\theta$ cannot appear because of the symmetry between the two protons. In the experiments done so far, terms higher than $\cos^2\theta$ have not been needed to fit the data.

Prokoshkin and Tiapkin found that at 445 MeV, $b \approx 1$, i.e., approximately equal numbers of pions were distributed isotropically and with a $\cos^2\theta$ distribution.[22] At 660 MeV they find that the distribution has become isotropic. In contrast to this, Dunaitsev and Prokoshkin find that the pions are produced isotropically over the entire region from 400 to 660 MeV.[23] The results of

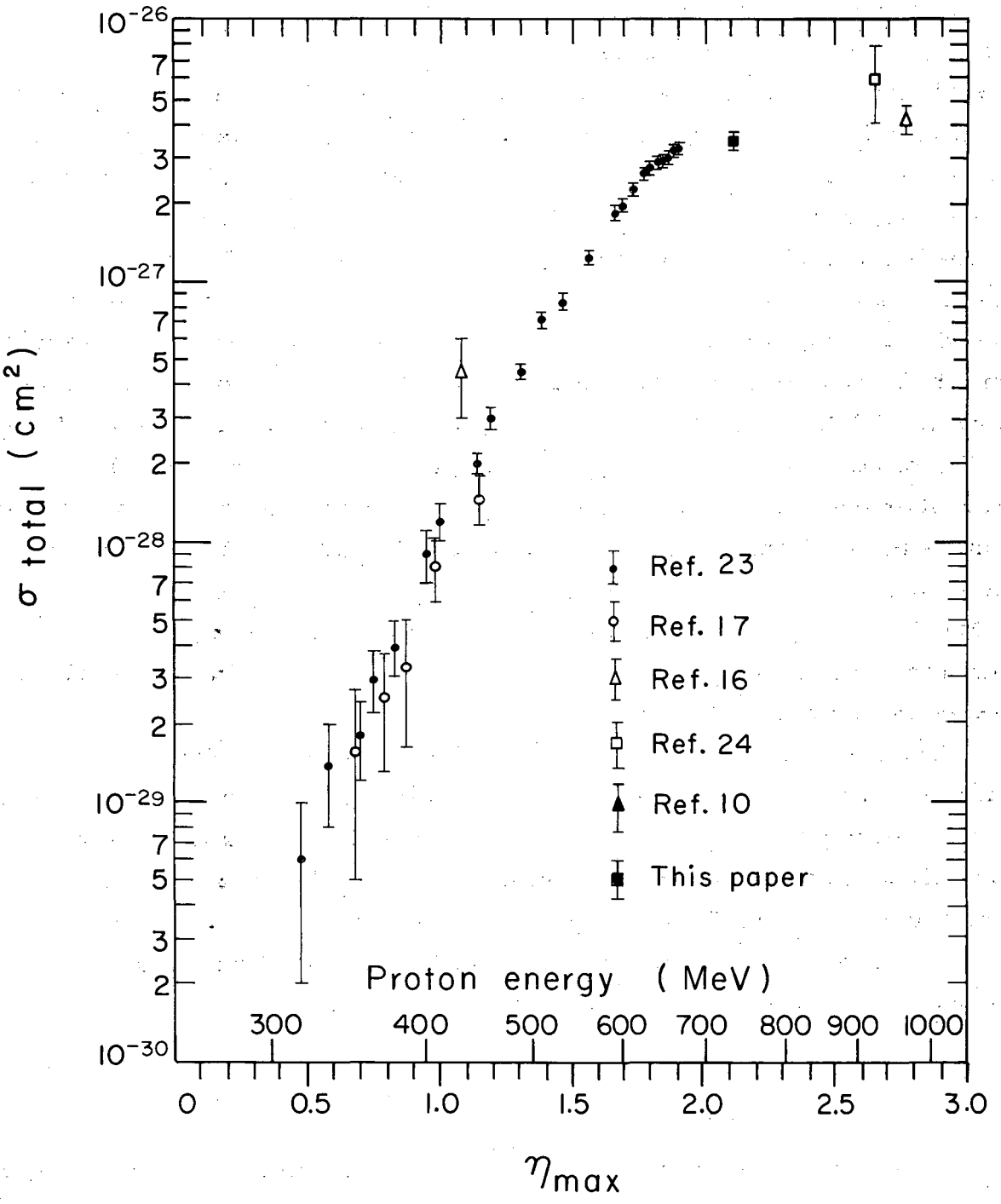

Fig. 1. Total cross section for the reaction $p + p \rightarrow p + p + \pi^0$. The abscissa is η_{max}, the maximum pion momentum in the c.m. system, in units of $m_{\pi^0}c$.

York et al. at 397 to 445 MeV[18] are also consistent with isotropic production. The only experiment on hydrogen done with a pair spectrometer finds $b = 0.1 \pm 0.03$ at 660 MeV.[25] It is interesting to note that Mandelstam's resonance theory predicts almost complete isotropy at all energies to 700 MeV.[6, 23]

Information on pion-energy distributions is almost nonexistent. One must have accurate gamma-ray spectra at several angles of view to obtain this information, and this has simply not been available. Baiukov and Tiapkin find that at 660 MeV the most probable π^0 energy is about 0.45 times the maximum available.[25]

Several experiments in the BeV region by Collins et al. have measured the energy spectrum of the recoil protons in p-p collisions.[26, 27] They found strong peaks in the spectrum of the unexcited proton when a nuclear isobar is formed:

$$p + p \rightarrow p + p^{*}.$$

The principal peak occurs at an energy corresponding to about 1.20 BeV for the isobar, slightly less than the 1.23 BeV predicted from the isobar model. These experiments, of course, cannot distinguish between π^0 and π^+ production.

C. Motivation for this Experiment

Several conclusions may be drawn from a review of the experiments which have been performed so far on the $p + p \rightarrow p + p + \pi^0$ reaction:

(a) With the exception of the total cross-section measurements, we have very little accurate information about the reaction, at any energy.

(b) Most of the experiments measured only gamma-ray fluxes, and did not measure energy spectra. Unless we know the gamma-ray energies, only limited information can be derived.

(c) The only experiment that used a pair spectrometer for accurate energy measurements used internal cyclotron targets and a $C - CH_2$ difference technique.[25] Because of the experimental difficulties, the results had large statistical errors.

(d) Almost no information, except for total cross section, has been obtained at any energy above 660 MeV. More accurate information at higher energies is needed to adequately test the isobar and peripheral interaction models.

(e) All experiments have assumed the only source of gamma rays at cyclotron energies is from π^0 decay. This hypothesis can only be tested by a detailed

investigation of gamma-ray spectra at several angles. This has been done only with carbon targets,[19, 28] where the center of mass is indeterminate.

In light of these considerations, we decided to conduct an experiment using the external 735-MeV proton beam from the Berkeley cyclotron, a liquid hydrogen target, and a high-energy precision pair spectrometer. We wished to measure the fluxes and energy spectra of the gamma quanta from the target at three carefully selected angles. From this information we hoped to answer the following questions:

(a) Do all the gamma rays arise from π^0 decay, or are there some of non-π^0 origin?

(b) What is the total cross section for π^0 production at 735 MeV?

(c) What is the angular distribution of π^0 mesons produced in the c.m. system?

(d) What is the momentum distribution of the neutral pions at different c.m. angles?

(e) How do the answers to these questions compare with the predictions of the various current theories of meson production?

Spectra were measured at three laboratory angles with respect to the incoming proton beam: at 6, 32, and 60 deg. These correspond to c.m. angles of 11, 55, and 93 deg. Since the beam is unpolarized and the protons are identical, all measured experimental quantities must be symmetrical about the 90-deg plane in the center of mass. We therefore also have effective information at 125 and 169 deg in the c.m. frame.

One may use certain symmetry arguments to predict several things about the gamma-ray spectra. Let us assume that the spectra are plotted in the c.m. system such that the energy scale is logarithmic (see Fig. 2). We draw a vertical line at an energy equal to half the π^0 rest mass (67.5 MeV). If the gamma rays are assumed to come only from π^0 decay, the following statements can be proved (see Appendix F, and references 19, 29, and 30):

(a) The total spectrum (that is, the spectrum integrated over all angles) is geometrically symmetric about the 67.5-MeV vertical line. That is, a cutoff at the high-energy end is matched by an equidistant low-energy cutoff. The shape of the spectrum above 67.5 MeV is exactly the same as the shape below 67.5 MeV. In particular, the peak of the spectrum must lie at 67.5 MeV. These statements hold true for the total spectrum in any coordinate system, whether or not it is the center-of-mass system.

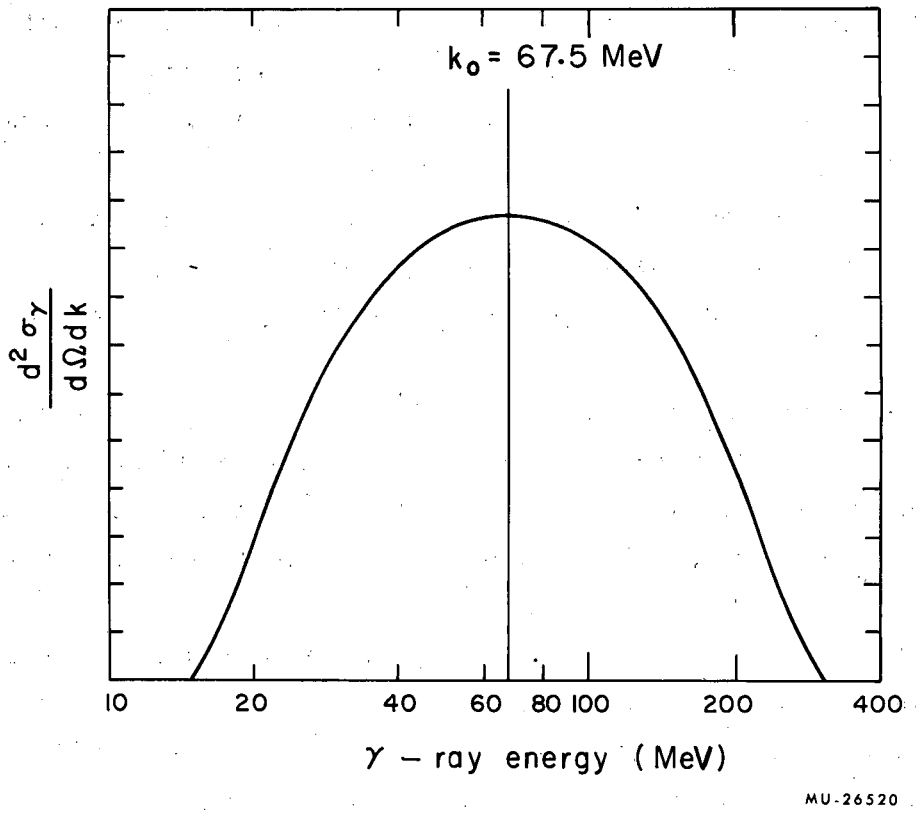

Fig. 2. Illustration of the symmetry properties of the gamma-ray spectra.

(b) The same symmetry properties hold true for the c. m. spectrum at the so-called "isotropic" angle, $\theta_{c.m.} = 55$ deg, for which $\cos^2\theta_{c.m.} = 1/3$, so long as there are only isotropic and $\cos^2\theta$ terms in the π^0 angular distribution. If there are higher terms with positive coefficients, then the peak of the gamma-ray spectrum is shifted to a slightly higher energy.

(c) At angles between 0 and 55 deg, the peak of the spectrum will be shifted above 67.5 MeV if there are positive terms in the pion angular distribution proportional to $\cos^2\theta_{c.m.}$. At angles between 55 and 125 deg the peak will be below 67.5 MeV. See Fig. 25 in Appendix F.

(d) The total cross section may be determined by a single measurement of the gamma-ray flux at the isotropic angle (again assuming no terms higher than $\cos^2\theta_{c.m.}$). Measurements at other angles are unnecessary for total cross section.

By using this information, we can gain a great deal of qualitative information from a cursory examination of an experimental spectrum. More detailed information on pion angular and energy distributions, however, can only come from a detailed comparison of the spectra with the kinematic theory as developed in Appendix F.

The next section reviews the experimental method and describes the apparatus used. Section III describes the methods developed to analyze the raw experimental data to obtain gamma-ray spectra. Section IV gives the experimental results and the π^0 distributions obtained from these results. Section V compares these results with current theories and gives a summary and conclusion.

II. EXPERIMENTAL METHOD

A. Introduction

The basic objective of this experiment was to measure the spectra of gamma rays emerging from a liquid hydrogen target bombarded with 735-MeV protons at three laboratory angles with respect to the incoming protons: 6, 32, and 60 deg. At this energy, gamma rays from π^0 decay can be produced from around 20 MeV up to a maximum of 540 MeV. Instruments therefore had to be constructed which could detect gamma rays over a very broad range of energies, with efficiencies known accurately over the entire range. To obtain the desired range, accuracy, and resolution, we used two pair spectrometers. A third spectrometer constructed in the early stages of the experiment was found unsatisfactory for reasons to be discussed, and the data obtained from it was not used in the final analysis.

The spectrometer is based on fairly simple and straightforward principles, and the electromagnetic interactions involved are well understood theoretically. Efficiencies and resolution functions can therefore be calculated with reasonable confidence. In simplest terms, a thin target of high-Z material, called a converter or radiator, is placed in the path of the beam of gamma rays to be analyzed. Some of the gamma rays will give up their energies in the converter to produce electron-positron pairs, which emerge in a small cone in the forward direction. The electrons and positrons travel through a magnetic field and are deflected in opposite directions. They are then detected by a series of scintillators placed on both sides of the magnet. Knowing the magnetic field, one can determine the energy of the particles; the sum of the two energies (including rest masses) equals the energy of the gamma ray.

Part B of this section will discuss the physical layouts used to measure the spectra at three angles, and will also discuss the characteristics of the proton beam. Part C will discuss the three spectrometers that were used, along with some of the attendant apparatus. Part D will describe the electronics used to detect the coincidences and store the data. The last part outlines the experimental procedures used during the run.

B. Physical Layout

1. Cave Layout

The layout of the hydrogen target and magnets to achieve the three desired angles is shown in Figs. 3(A), 3(B), and 3(C). In all cases the proton beam remained inside the physics cave, and the gamma rays were viewed from outside the cave through a port built into the wall of the physics cave. The 60-deg angle was the easiest to obtain, since it was not necessary to bend the proton beam at all. The 6-deg angle was the most difficult; two magnets were necessary to bend the beam toward one of the ports, then a third to deflect it back again.

Figure 4 shows a typical layout along the gamma-ray channel. M_1 and M_2 are sweeping magnets used to separate charged particles, primarily π^+ mesons, from the gamma rays. An anticoincidence counter, described below, was placed in front of the spectrometer in order to further reduce charged particle background. Its main effect was to significantly improve the converter in-out ratio.

2. Proton Beam

The external proton beam of the 184-inch cyclotron emerges into the physics cave with a mean energy of approximately 740 MeV. Von Friesen and Barkas,[31] and Larsen,[32] have made extensive studies of its characteristics. Figure 5 shows the relationship of the physics cave to the cyclotron itself. By varying the current in the internal quadrupole and steering magnet, we were able to obtain a beam spot approximately two inches in diameter, with a maximum current of 0.03 μa, or 2×10^{11} protons/sec. Through use of the auxiliary dee, this beam could be spilled out evenly over a period of about eight msec, giving a duty cycle of approximately 50%.

The proton beam was monitored by means of a secondary emission chamber, or SEM chamber, similar to that used by Larsen.[32] An ion chamber was also used to monitor the beam, but gave evidence of substantial saturation effects at the beam currents which were used. A careful check of the operational characteristics of SEM, however, indicated no evidence of nonlinearity.

A proton beam produces current in a secondary emission chamber by knocking ions out of a series of thin aluminum plates, rather than by ionization of the gas through which it passes as in a normal ion chamber. Since an ion chamber produces over a thousand times as much current as a SEM

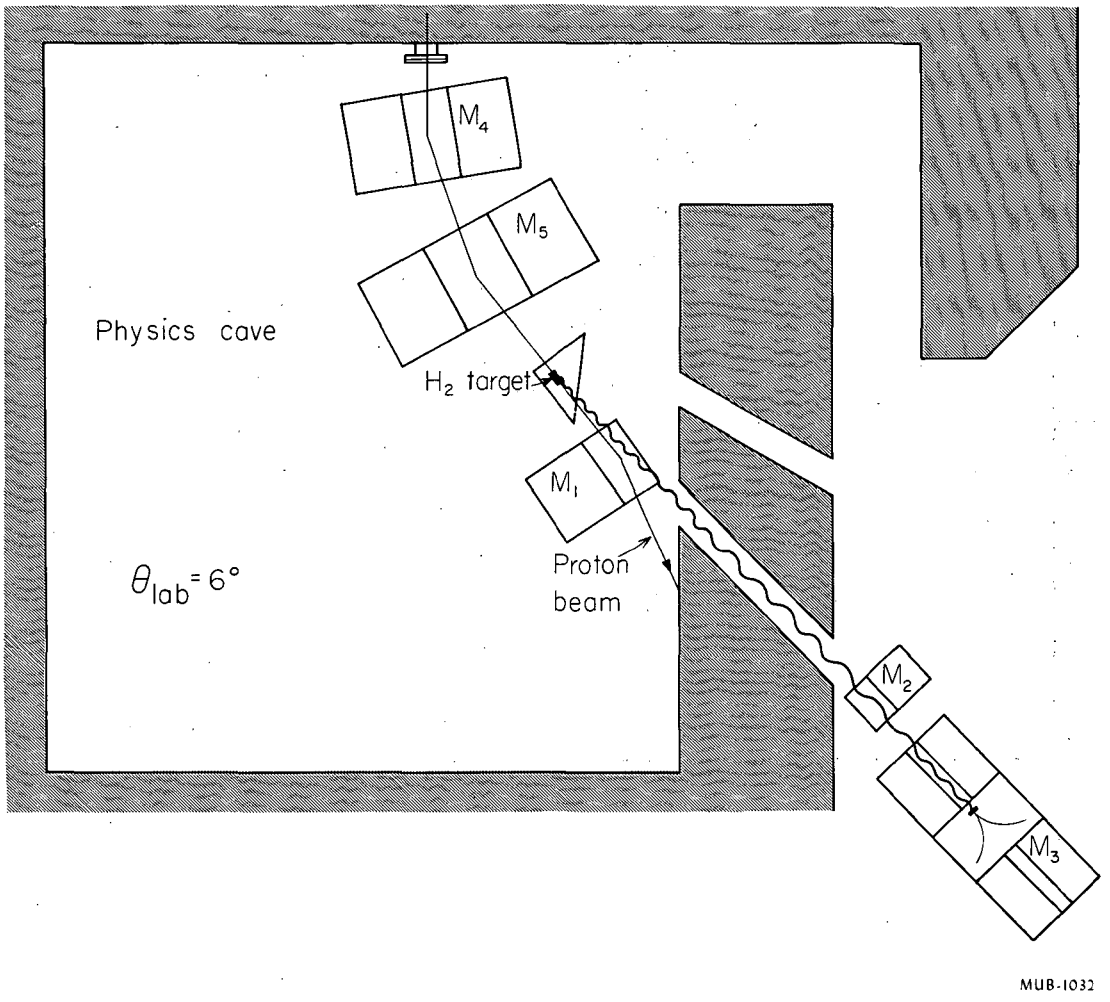

Fig. 3(A). Beam setup at 6 deg lab. M_1 and M_2 act as sweeping magnets and M_3 is the spectrometer magnet; M_4, M_5, and M_1 guide the proton beam.

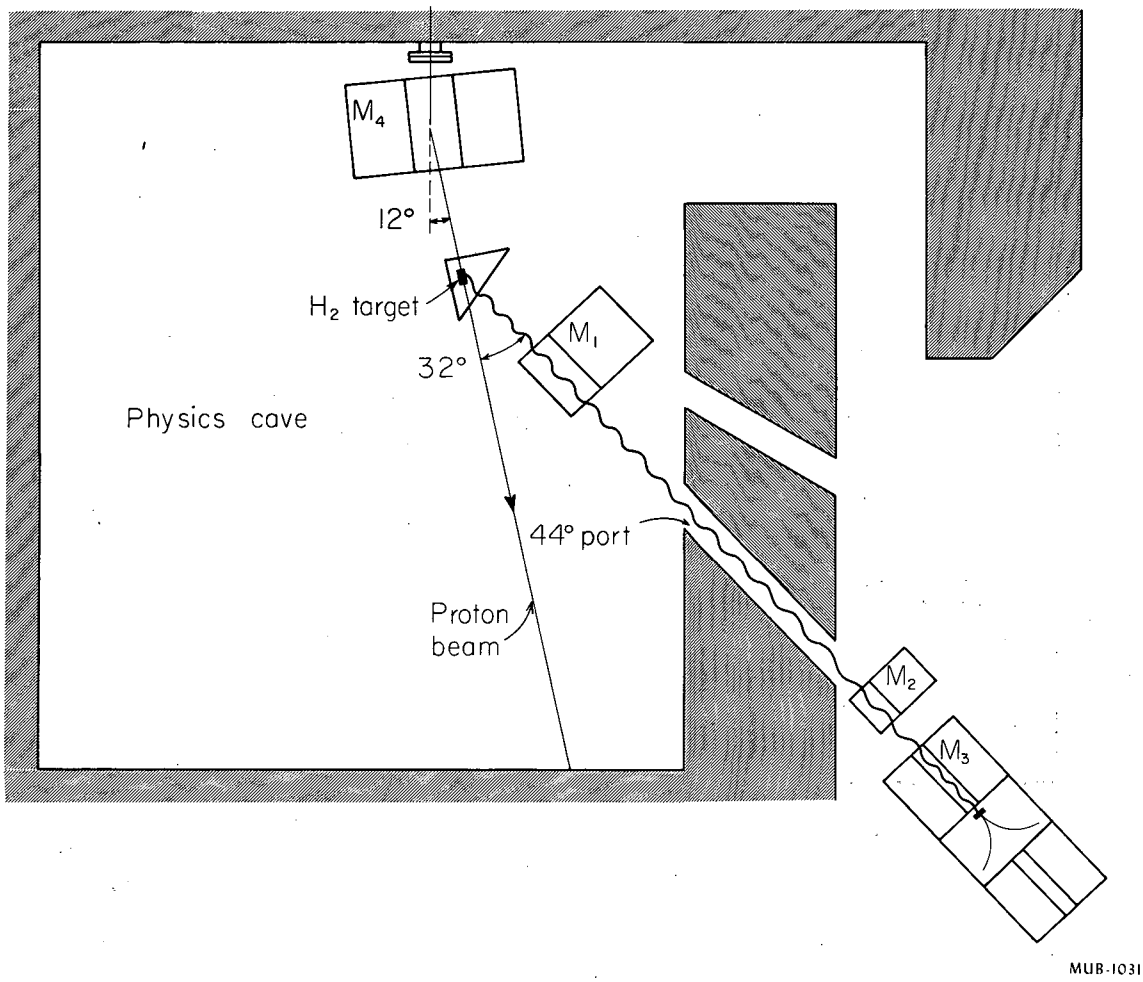

Fig. 3(B). Beam setup at 32 deg lab. M_1 and M_2 are sweeping magnets.

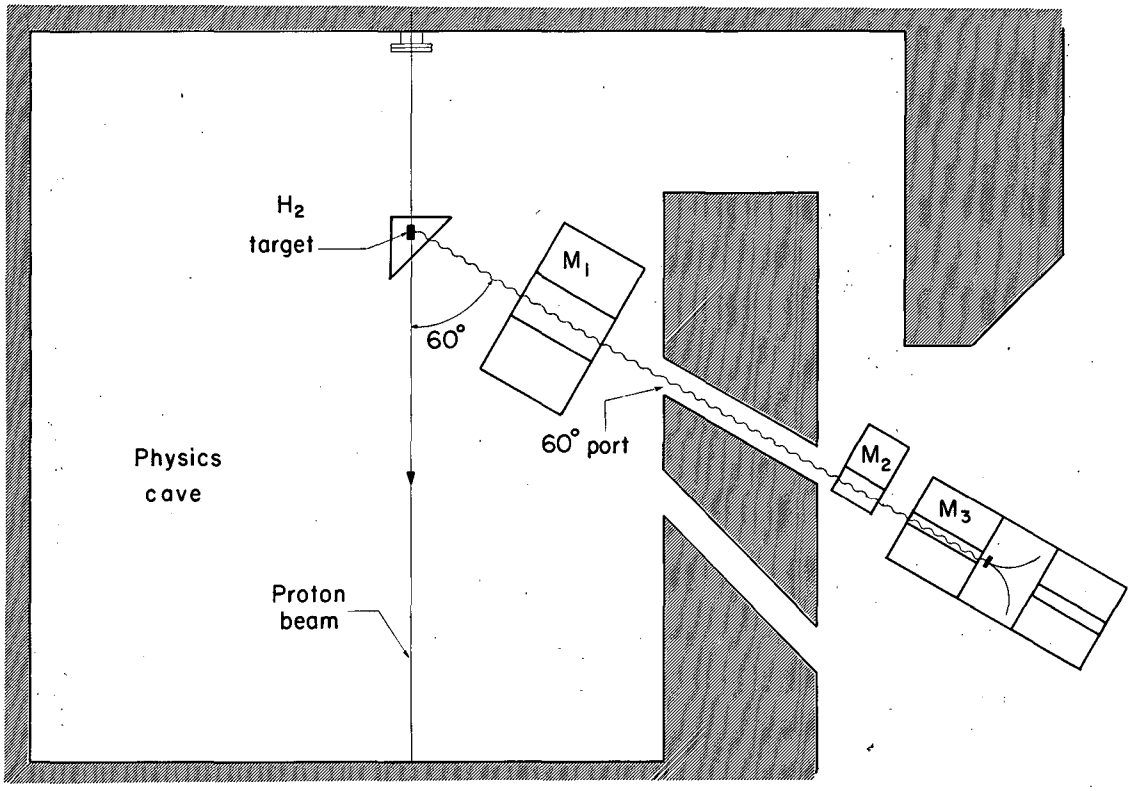

Fig. 3(C). Beam setup at 60 deg lab.

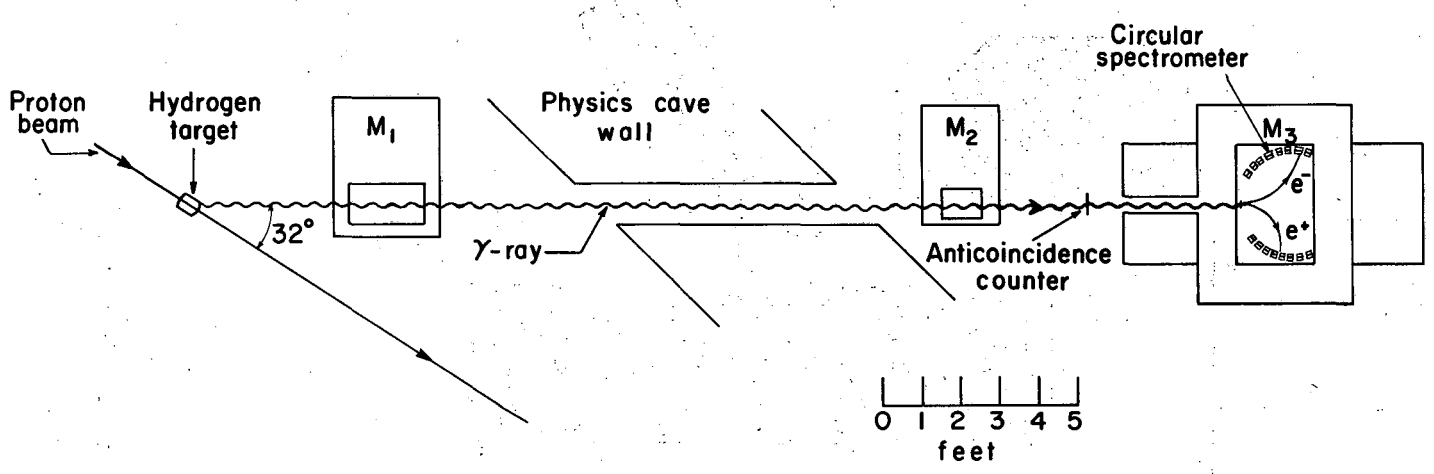

Fig. 4. Typical layout along the γ-ray channel. M_1 and M_2 are sweeping magnets. The anticoincidence counter detects any remaining charged particles.

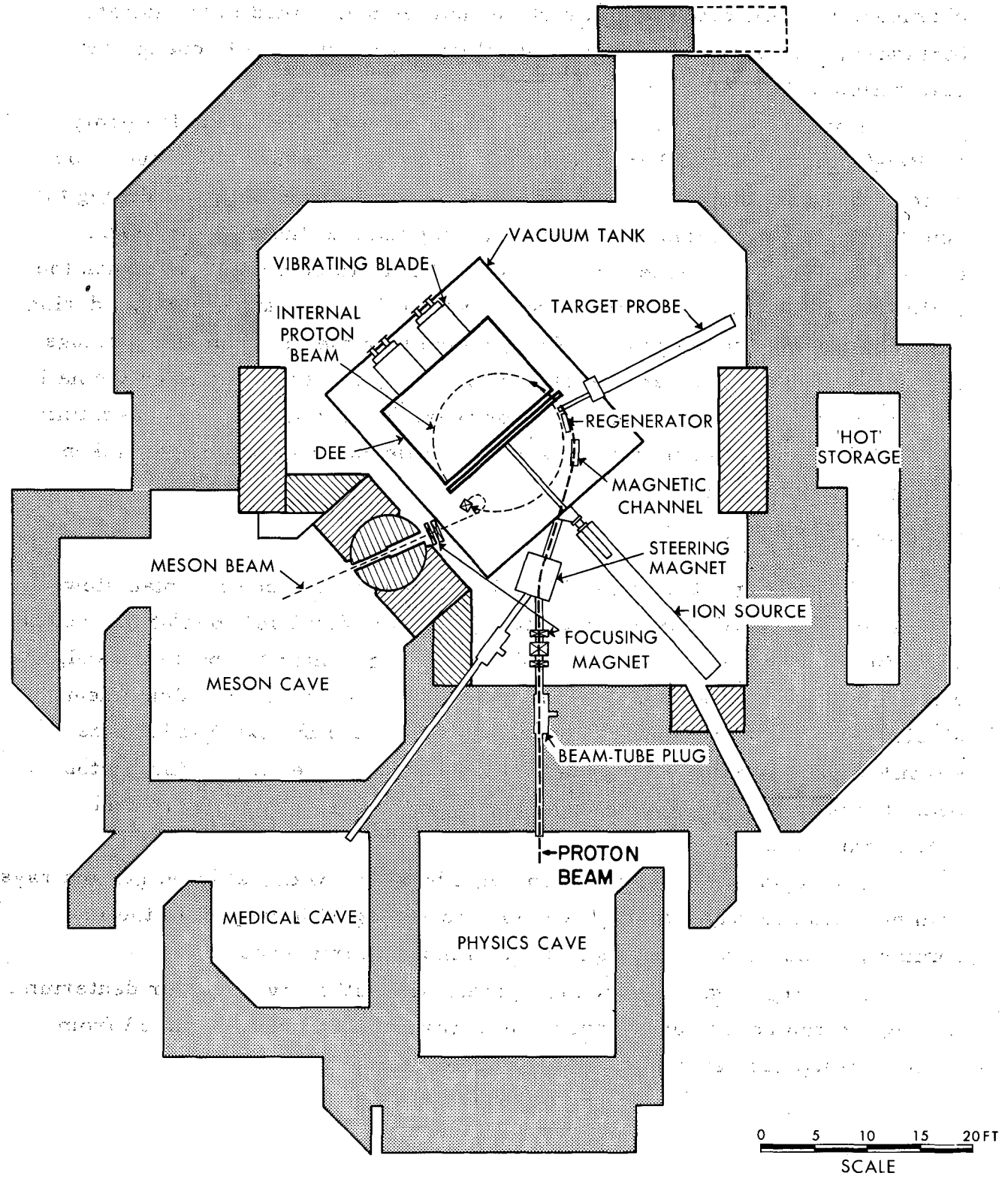

Fig. 5. Plan view of the 184-inch cyclotron, showing the physics cave.

chamber, it is important that a high vacuum be maintained in the latter; otherwise, the ionization of the residual gas will significantly change the calibration of the chamber.

A high vacuum was maintained by attaching a Varian VacIon pump (1 liter/sec) to the chamber. For the most part, pressures of about 1μ or better were maintained. However, it was discovered at one point during the run that the VacIon pump was malfunctioning and that the pressure in the chamber had risen considerably. It was difficult to determine just when the malfunctioning began, and the degree to which the calibration changed during this period was also uncertain. Comparison with the ion chamber readings gave some information, and repetition of runs gave assurance of only small change within any 24-hour period. However, there remained an uncertainty of about 5% in the overall normalization of different sections of data taken during the one-month run.

3. Hydrogen Target

The hydrogen target used in this experiment is shown in plan view in Fig. 6. The flask was a horizontal Mylar cylinder 6 in. long at the center and 5 in. in diameter. The end windows, through which the beam passed, were 9 mils thick. Surrounding the flask was a 1-1/2-mil aluminum heat shield. The entrance window was 25-mil Mylar and the exit window was 45-mil Mylar. Thus, in its passage through the entire target, the proton beam traversed 1.08 g/cm^2 of hydrogen, 0.02 g/cm^2 of aluminum, and 0.31 g/cm^2 of Mylar.

The Mylar exit window, 6 in. high by 27 in. wide, allowed gamma rays coming from the target at angles from 0 to 90 deg with respect to the incoming protons to pass through with minimum interference.

The target was designed to operate with either hydrogen or deuterium. During the run both liquids were used as targets. The data obtained from deuterium will be reported in a later publication.

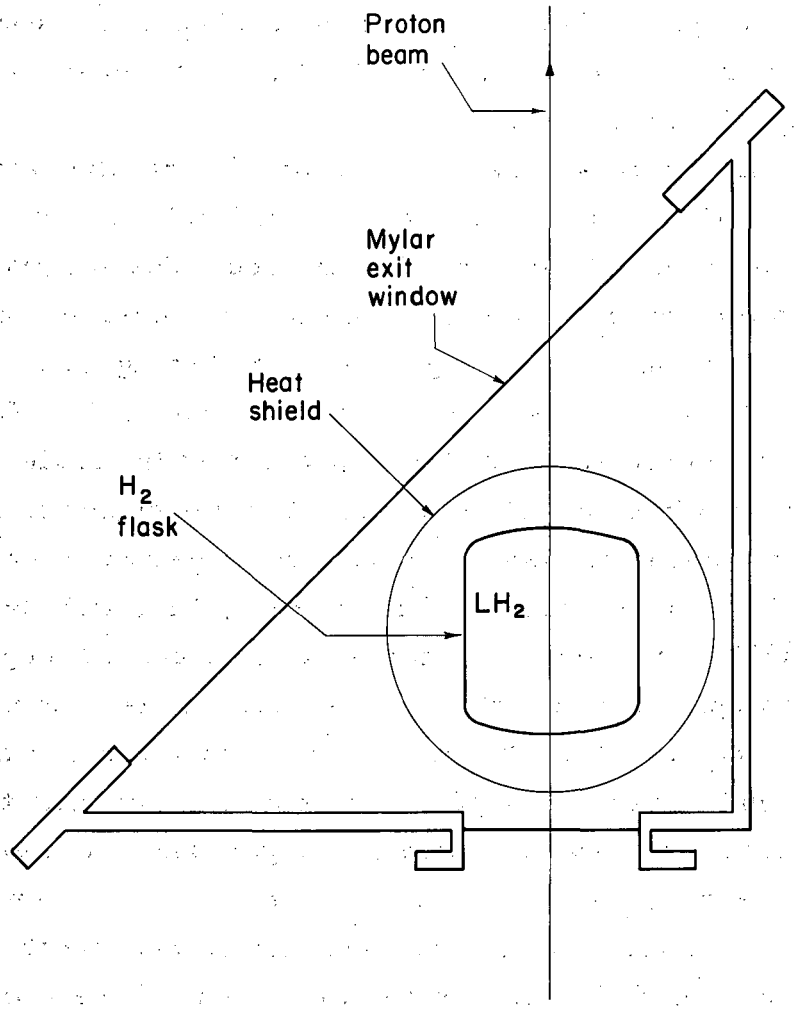

Fig. 6. Plan view of the liquid hydrogen target. The flask was 6 in. long at the center. The wide exit window permitted viewing the γ rays at any angle from 0 to 90 deg.

C. Physical Apparatus

1. Spectrometers

The design, development, and construction of the spectrometers for this experiment took place over a period of more than three years. Three different spectrometers were designed and built. Data obtained from only the last two were used in the final analysis.

All three instruments were designed for use with the same analyzing magnet, "Orion." This magnet has 24-in. × 36-in. pole pieces, over which a uniform field of up to 20,000 gauss can be obtained. Special yoke pieces were built to enable gamma rays to enter the field in a direction perpendicular to the longest pole dimension. A 5-in. gap was used throughout.

The geometry of the first spectrometer is indicated in Fig. 7. We called this the "74-degree spectrometer," because of the angle between the converter and the two lines of scintillators. It was designed to cover gamma-ray energies up to 650 MeV. Two versions of this spectrometer were used. The first used plastic scintillators 1/2 in. thick by 1 in. wide by 2 in. high, joined to RCA 6810A photomultiplier tubes by clear curved lengths of Lucite, designed to follow approximately the expected path of the electrons. The phototubes were located in the horizontal plane, about a foot away from the pole pieces. The second version differed in two respects. Scintillators 4 in. high replaced the earlier ones, so as to detect a larger fraction of electrons undergoing vertical scattering in the converter. Also, hollow aluminum light pipes replaced the earlier Lucite ones, so as to eliminate what we thought might be Čerenkov radiation caused by electrons scattered out of one scintillator into an adjacent light pipe.

Both of these versions suffered from a common defect. Often when a coincidence occurred, two or more counters on the same side, usually adjacent, produced a signal simultaneously, as though a single electron had gone through two or more scintillators. Multiple coincidences of this type occurred as much as 10% of the time, and seemed to be more prevalent at the higher magnetic fields.

We never fully understood the basis for this phenomenon. One possibility is that electron-electron collisions in the scintillator produce delta rays of lower energy, which are then able to circle back into an adjacent scintillator. However, calculations based on this assumption indicate that

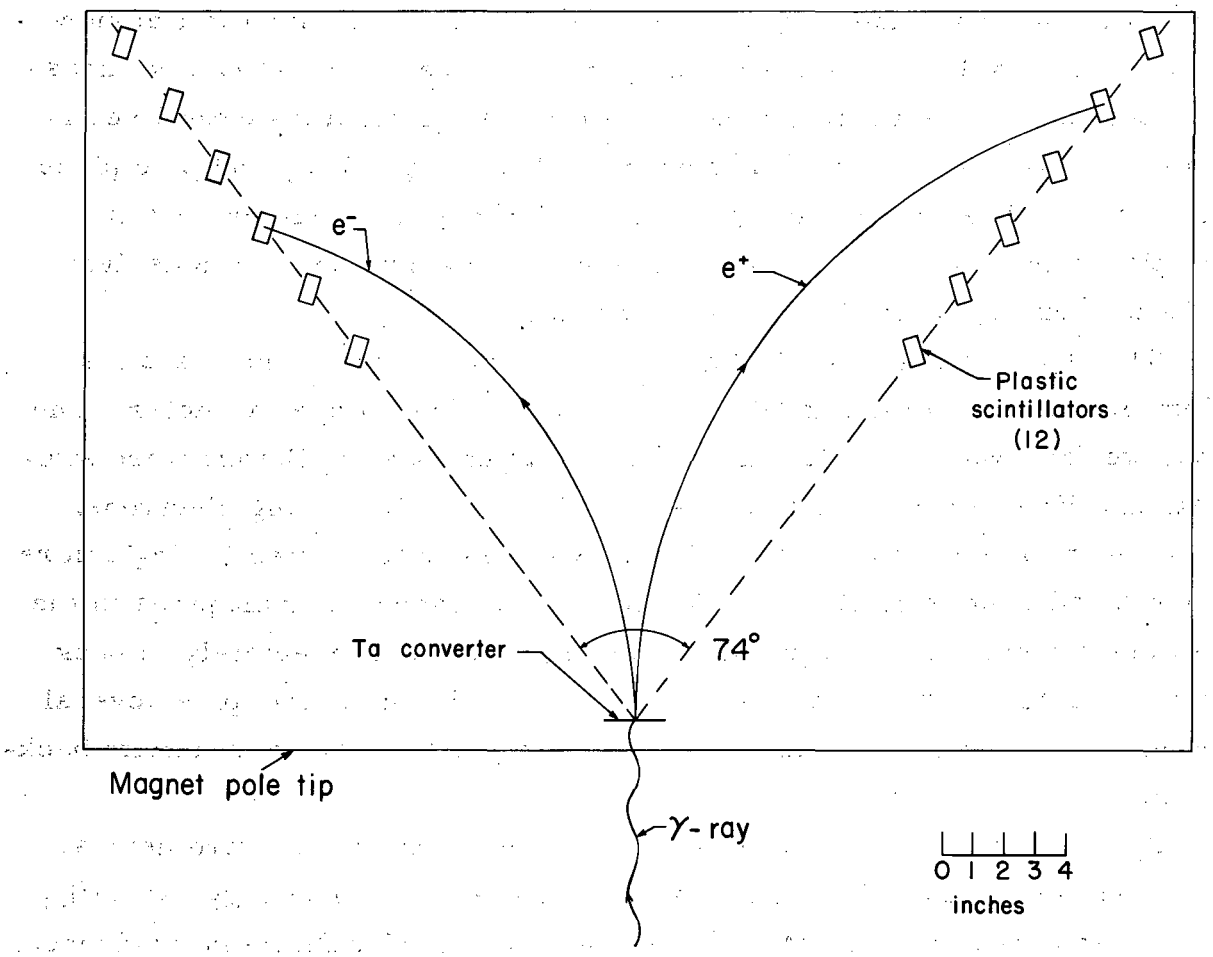

Fig. 7. The 74-deg spectrometer. This was found to be unsatisfactory, for reasons discussed in the text.

the probability for this process is somewhat less than that needed to explain the results. A second possibility is that somehow electrons could scatter from one scintillator to an adjacent one.

The geometry of the second spectrometer is shown in Fig. 8. This was designed especially for the lower-energy region of the spectrum, and is a conventional 180-deg spectrometer. Six scintillators on each side, each 1/2 in. thick by 1 in. wide by 4 in. high, detect electrons with radii of curvature from 3 in. to 8 in. The maximum gamma-ray energy that can be measured is 240 MeV. Lucite light pipes joined to the scintillators extend vertically through 2-in.-diam holes drilled through the upper body and pole piece of the magnet. The 6810A photomultipliers and magnetic shields rest on stands placed on top of the magnet. Thus only the scintillators themselves, plus the converter, lie in the median horizontal plane.

This spectrometer worked quite satisfactorily and did not have the problem of multiple coincidences exhibited by the 74-deg spectrometer. The reason, we felt, was two-fold. First of all, adjacent scintillators were situated along a line perpendicular to the direction of the impinging electrons. Thus an electron entering one scintillator would have to scatter 90 deg before reaching an adjacent scintillator. Secondly, the absence of light pipes in the median plane permitted us to place absorbing material immediately in back of the scintillators. We used a block of 1-in.-thick aluminum, plus several layers of lead bricks. Aluminum was chosen so as to produce minimum backscattering.

After having experience with each of these first two spectrometers, we set about designing a third one that would have the high-energy capability of the 74-deg spectrometer, but without the problem of multiple coincidences. We felt this could best be accomplished by incorporating some of the basic design characteristics of the 180-deg spectrometer, but with much larger electron-radii of curvature. In particular, we required that light pipes extend vertically through holes drilled in the magnet, and that adjacent scintillators lie along a line perpendicular to the electron direction. This led to a design with the geometry shown in Fig. 9. Here the converter and all scintillators lie on the circumference of a circle of 16-in. radius. Eight scintillators on a side are each 1/2 in. thick and 4 in. high, but have variable widths. The energy resolution of a spectrometer is given primarily by the widths of the detectors (see Appendix B): our widths were chosen so as to keep the percentage

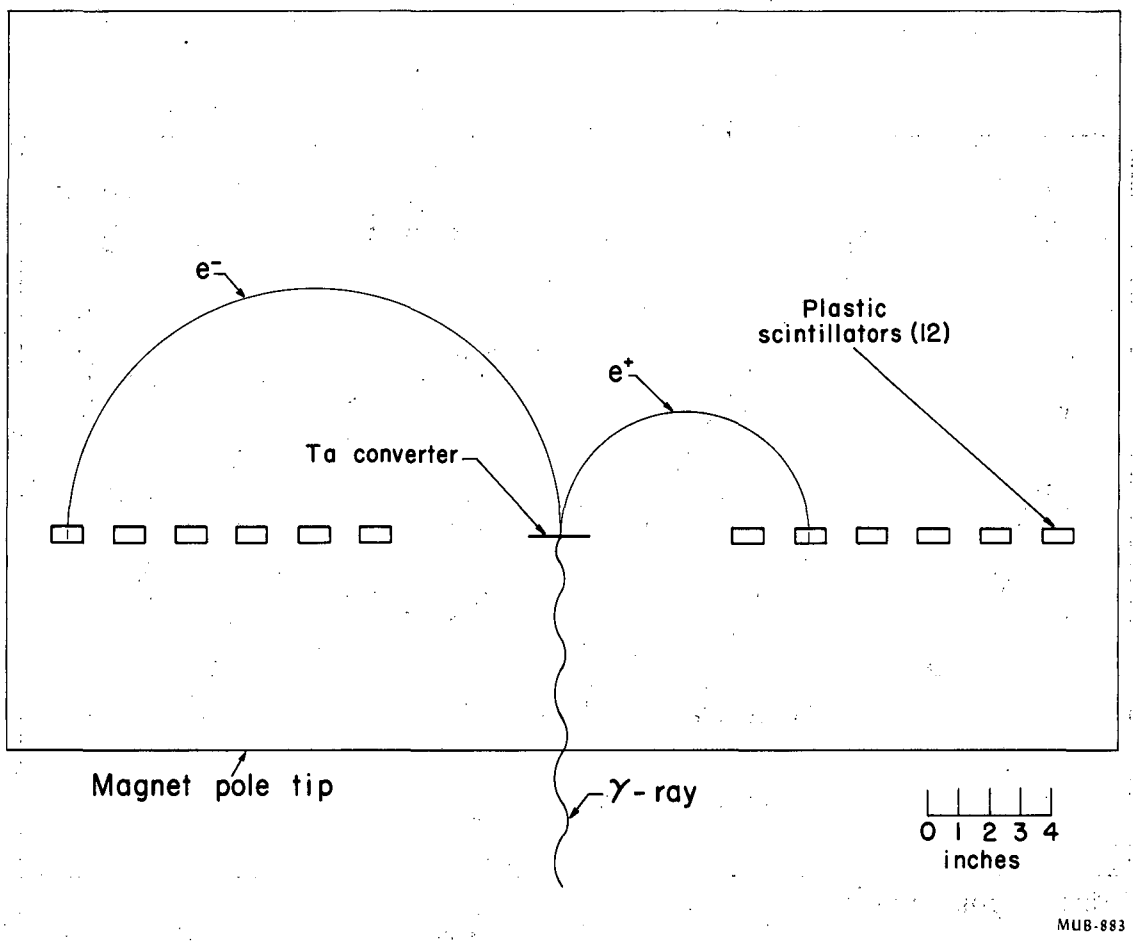

Fig. 8. The 180-deg spectrometer. Maximum γ-ray energy is 240 MeV.

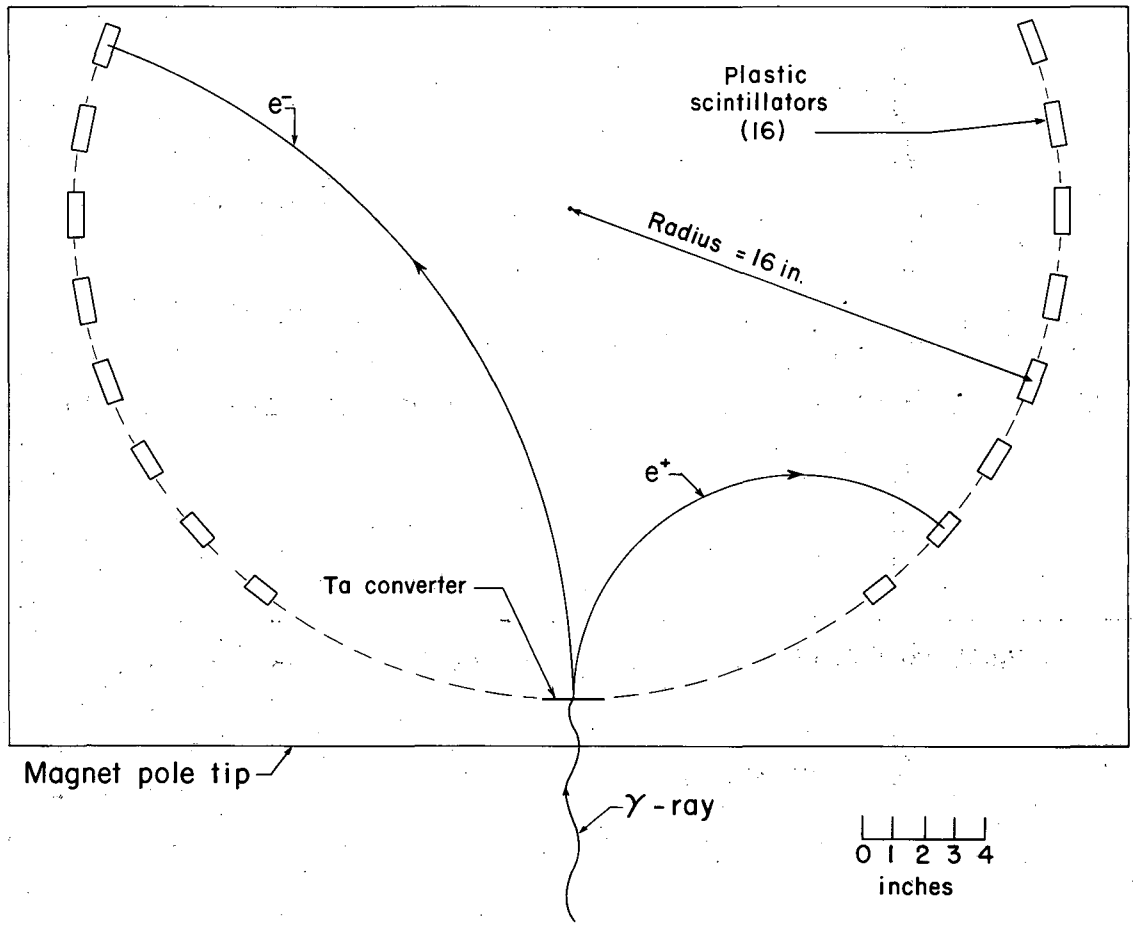

Fig. 9. The circular spectrometer. Gamma rays up to 650 MeV can be analyzed. The variable counter widths ensure a uniform percentage resolution.

resolution a constant for each detector. By varying the actual widths from 0.94 in. to 1.50 in., uniform resolutions of 10% (full width) of the electron energy were attained. In contrast, the electron energy resolutions of the 180-deg spectrometer ranged from 7% to 17%.

This third spectrometer, which we refer to as the circular spectrometer, worked extremely well. Gamma-ray energies up to 650 MeV can be measured. As in the case of the 180-deg spectrometer, the scintillators were backed up with 1 in. of aluminum and several layers of lead. Multiple coincidences were negligible. The overall counting efficiency was several times as great as that of the 74-deg spectrometer, for two reasons. First, there were eight detectors on each side instead of six. Also, each detector was on the average wider, and therefore a larger fraction of the electrons were detected. Since the overall gamma-ray efficiency goes as the square of the efficiency for detecting electrons or positrons, these factors were significant. Under typical running conditions with a hydrogen target at the 6-deg laboratory angle, as many as 4,000 gamma rays per minute were analyzed.

A converter flipper was designed to use with either the 180-deg or the circular spectrometer, which could be remotely controlled from the counting area. This is pictured in Fig. 10. A converter is attached to a thin piece of Mylar, which is in turn attached to a Micarta frame. A similar piece of Mylar, with no converter, is attached to another frame in a plane perpendicular to the plane of the first frame. These two frames are rigid with respect to each other, but can rotate together through a 90-deg angle. Several turns of thin wire wrapped around each frame form a current loop. When current flows through the wire, the frames, situated in a magnetic field, tend to rotate so as to maximize the number of lines of force passing through the current loop. Reversal of the current causes a rotation in the opposite direction. The figure shows the converter flipper in a midway position. This unit worked well at all magnetic fields, and saved a good deal of beam time which would have been lost if manual switching were necessary.

The choice of converters used depended upon the energies of the gamma rays being measured. Multiple scattering in the converter can cause electrons to be scattered vertically out of the plane of the detectors. The converters must be thin enough so that the loss of efficiency due to this scattering is not excessive. Since the average scattering angle is a strong function of

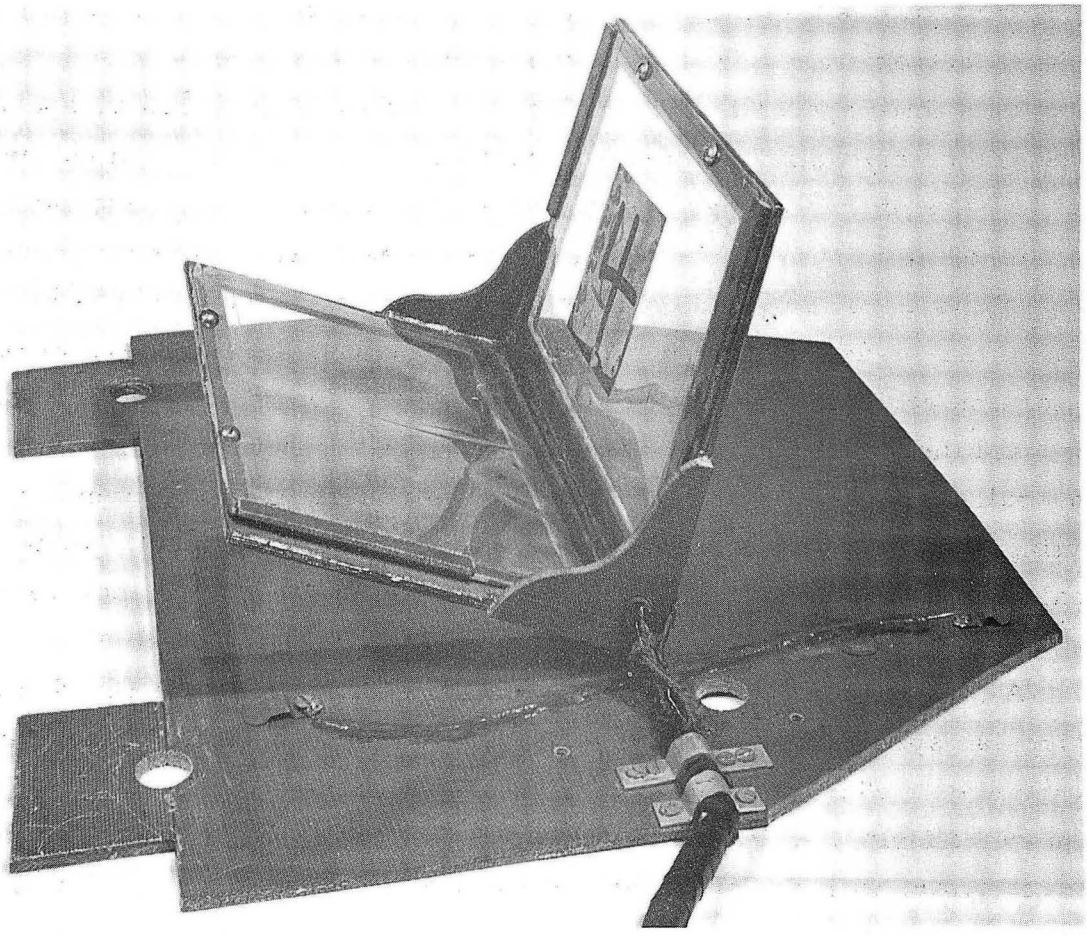

ZN-3236

Fig. 10. The converter flipper. A d. c. current flowing through loops of wire in the frame interacts with the magnetic field so as to orient the converter in either the in or the out position.

electron energy, thicker converters can safely be used when analyzing the higher-energy gamma rays. During our final run, for the circular spectrometer we used a tantalum converter 10 mils (0.010 in.) thick, with some data at lower current settings taken with a 4-mil converter. The 180-deg spectrometer used a 4-mil and a 2-mil converter. In no case were losses in overall efficiency due to vertical scattering greater than 50%, and over most of the region scattering losses were less than 20%. The effects of horizontal scattering, which broaden the energy resolution function, were negligible (see Appendix B). All converters were approximately 2 in. square. Thicknesses ranged from 0.090 to 0.410 g/cm^2 of tantalum.

After much experience with a number of different spectrometer designs, we felt that the circular spectrometer was the most effective instrument for our purposes. It had high efficiency and good resolution. It could analyze gamma rays over a very wide range of energies. It was easy to set up and tear down. Because the median plane was free of all apparatus except the scintillators themselves, it was easy to shield from extraneous radiation. If we were to perform a similar experiment in the future, we would probably use only this instrument. Analysis of low-energy gamma rays could be accomplished by using thinner converters and lower magnet currents. Although the geometric design at first glance seems highly unusual, its characteristics can be precisely calculated and the experimental data readily interpreted.

2. Anticoincidence Counter

One of the problems encountered in the early phases of the experiment had to do with production of showers in the gamma-ray channel. It is impossible to collimate a beam of high-energy gamma rays without the collimator itself acting as a target for pair production and bremsstrahlung. As a result some of the gamma rays striking the edge of the collimator produce a shower of electrons and lower-energy gamma rays. The electrons can be removed with sweeping magnets, but the low-energy gamma rays remain to contaminate the measured spectrum. The effect in our case is to warp somewhat the low-energy part of the spectrum and make it difficult to observe the low-energy cutoff predicted by π^0 decay kinematics. We found also that the observed spectrum was somewhat dependent upon the way in which we collimated. It was impossible to run with no collimation, because of the sharp rise in converter-out coincidences and the resulting decrease in the converter in-out ratio.

On the other hand, too much lead collimation in certain places produced a sizable increase in the number of low-energy gamma rays observed.

Our basic approach to the solution of this problem was to attempt to detect bremsstrahlung and shower events near the collimator with a special counter. The signal from this counter would then be placed in anticoincidence with the signals from the electron counters. Thus only gammas which were not produced from electron bremsstrahlung would be analyzed.

With these goals in mind, an anticoincidence counter was designed and built. This is shown in plan view in Fig. 11. There are three sections: the pre-collimator, the "bear claws," and the thin counter. The bear claws consisted of a sandwich of layers of lead 1/4-in. thick alternating with plastic scintillator, so that a developing shower would have a maximum probability of being detected. The thin counter, which was a plastic scintillator 20 mils thick, detected any remaining charged particles passing through. Two 6810A phototubes were attached to the bear claws, and two to the thin counter. The signals were all added together and the resulting signal used in anticoincidence. The counter was placed about four feet from the converter.

The effectiveness of this counter was somewhat less than we had hoped for. First of all, the singles counting rate was extremely high, of the order of 10^7 counts/sec instantaneous. With a duty cycle of about 20%, one questioned its effectiveness in being able to "anti" out undesirable events. Secondly, its actual effect on the observed spectrum was not too significant. The main effect was to decrease the number of converter-out counts, and therefore increase the converter in-out ratio by as much as a factor of 2. This showed that there were electron-positron pairs being produced somewhere in the gamma-ray channel which were detected by the spectrometer. However, the converter-out subtraction would normally compensate for this.

The anticoincidence counter was used in taking all of the data except that at 60 deg. In a direct comparison with data taken without antcoincidence, there seemed to be some decrease of gamma rays at the lowest part of the spectrum. However, we were never able to obtain a complete cutoff of gamma rays at energies below that expected from π^0 decay. Our feeling was that those remaining were not produced in the target, but resulted from bremsstrahlung events inseparable from the original gamma rays. As a result, we do not place high confidence in that portion of the spectrum below 75 or 100 MeV. Fortunately, the statistics are already poorest in this region, and it is possible

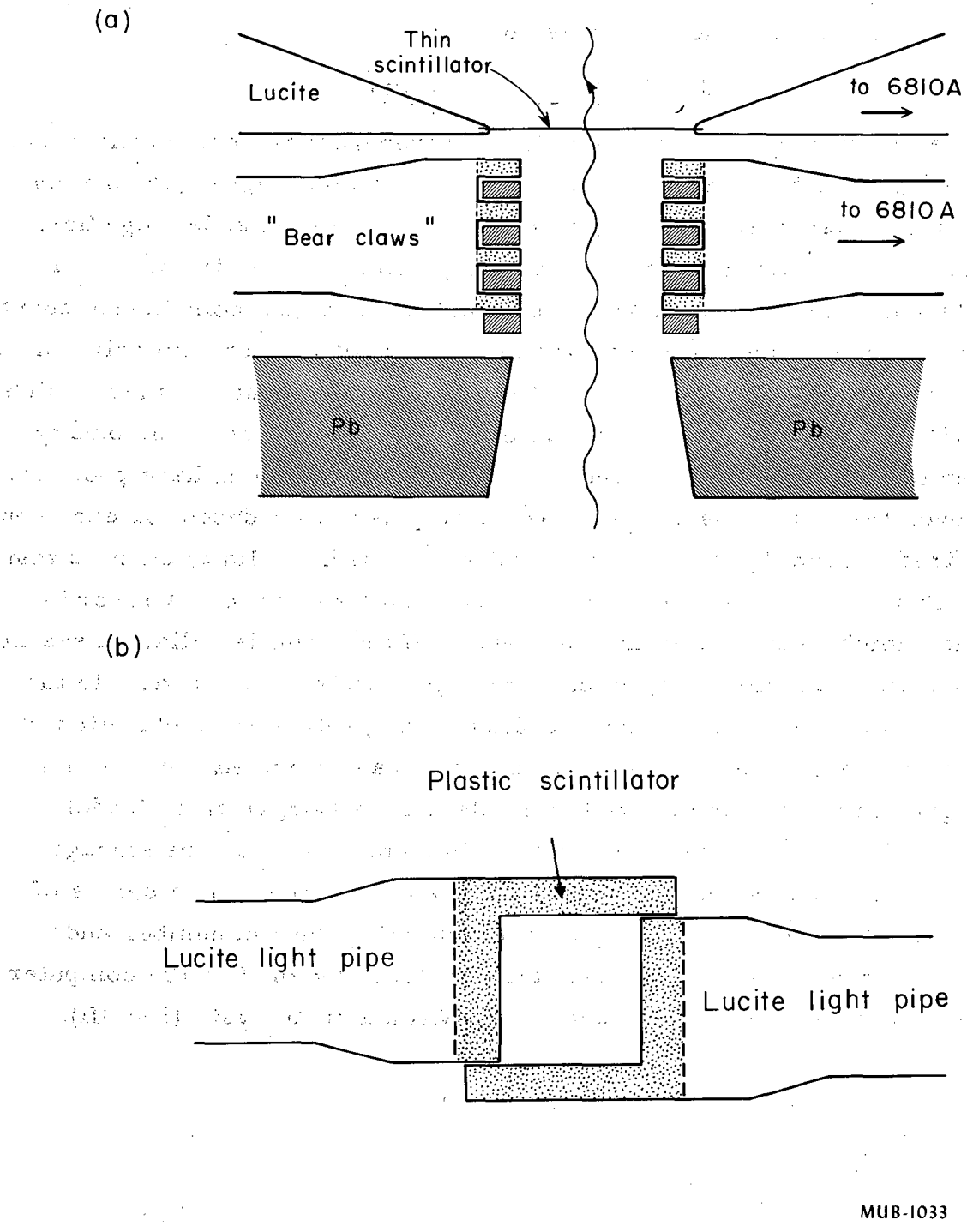

Fig. 11. The anticoincidence counter: (a) is a plan view, and (b) is a beam's-eye view. Shower events originating in any section of the lead collimator should be detected by one of the scintillators.

to make a unique determination of the π^0 energy and angular distribution without utilizing this part of the spectrum. The reader is referred to Sec. IV (Results) for further comments on this point.

D. Electronic Apparatus

The electronics used to determine electron-positron coincidences are shown in simplified block diagram in Fig. 12. The eight signals from each side (six in the case of the 180-deg spectrometer) are first added together. The summed signals are put into a Wenzel-type coincidence circuit[33] to determine two-fold coincidences, with the signal from the anticoincidence counter in anticoincidence. The resolving time of this circuit is approximately ten nsec (full width at half-max). The fast output triggers a gate former, which in turn informs the binary coder that an event has taken place. The binary coder then takes a "snapshot" of the particular counters which have produced a signal over the past 20 nsec. A square μsec pulse is produced for each counter that has fired. From here on μsec circuits are used. Validity circuits test to ensure that one and one counter only on each side has fired. A record is kept of the number and type of invalid events. If the event is valid, pulses in binary code are transmitted to the core storage matrix, which adds 1 to the number stored in the channel corresponding to the particular combination of counters that fired. The core storage unit is a transistorized 256-channel pulse-height analyzer manufactured by Nuclear Data Corporation, Model ND-101, which was modified for our use. On command, the core storage unit reads out the number of counts in each channel by punching a series of eight IBM cards, each prefaced by a code indicating the run number and running conditions. These cards are later analyzed by an IBM 709 computer, using a program described in the section on Method of Analysis (Sec. III).

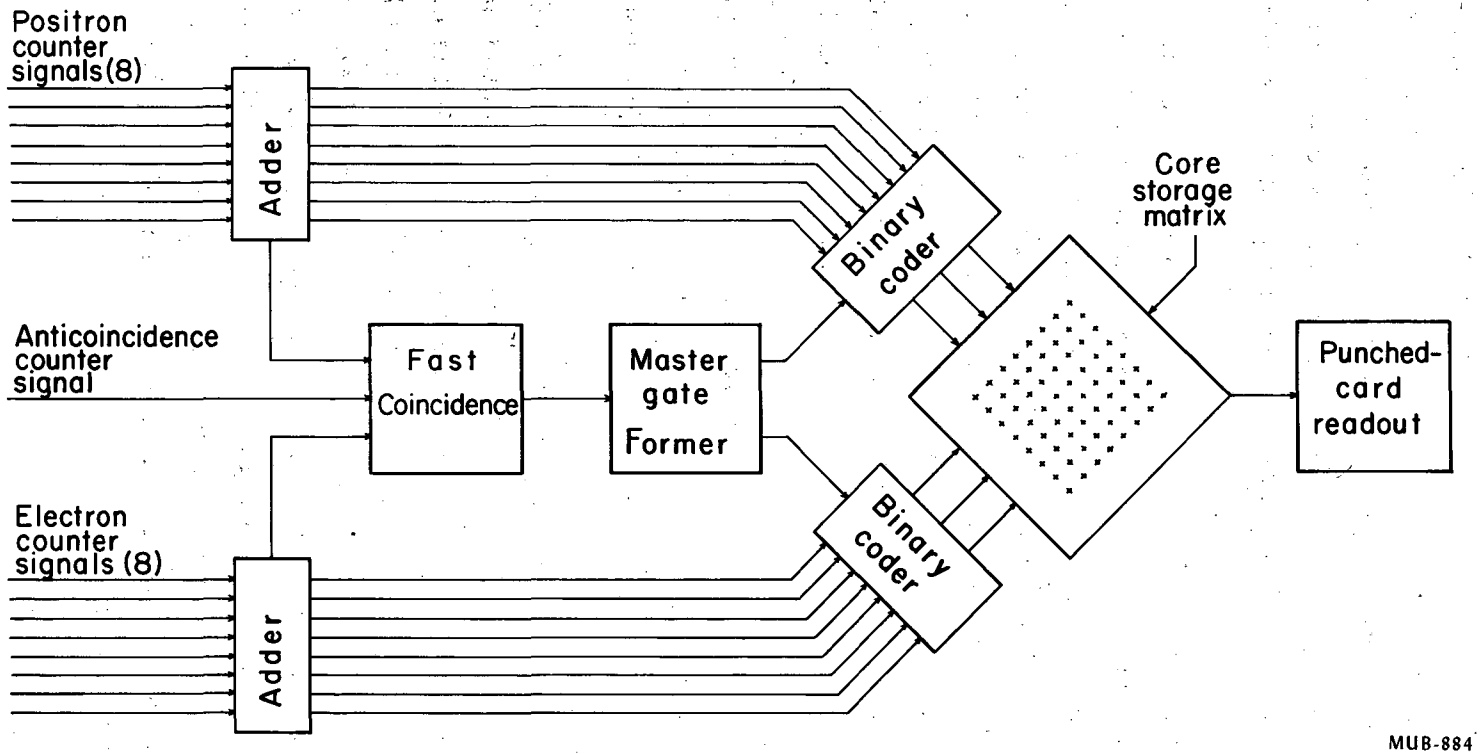

Fig. 12. Block diagram of the electronics. Fast circuits are used to the binary coder, and microsecond circuits from there on.

E. Experimental Procedures

Our final run at the cyclotron, during which time all the data reported here was taken, took place from March 25 to May 4, 1961. During this time we took data at the three lab angles of 6.2, 32.0, and 60.5 deg. At each angle, data was taken with hydrogen in the target, with deuterium, and with the target empty. Target in-out ratios of approximately 5:1 were obtained with hydrogen, and 12:1 with deuterium. The deuterium data will be analyzed separately and is not reported here.

Both the 180-deg and the circular spectrometer were used at all angles. For the most part, with each spectrometer we took data at each of 16 magnetic field settings, ranging from 1.92 to 19.7 kgauss. Each field setting differed from the previous one by a factor of 1.168; that is, equal increments of around 17% were chosen. The purpose of running at so many different fields was to average out the effect of possible small variations in efficiencies of individual counters or counter combinations. Discontinuities in observed spectra due to systematic variations in counter efficiencies are essentially eliminated if the value at each experimental point is determined by contributions from almost every possible counter combination. The data analysis becomes somewhat more complex, but we had committed ourselves at an early date to automatic data processing by computers, so that this decision presented no problem.

A run under a given set of conditions would typically take about 15 minutes; then we would turn off to punch out data. Time was allocated between converter-in and converter-out approximately as the square root of the counting rates (i.e., if the converter in-out ratio was 9:1, we ran three times as long on converter-in), in order to minimize the statistical error for a fixed amount of running time. The observed converter in-out ratios varied considerably, and depended on many factors, including magnet current, angle, collimation used, converter used, etc. Under some conditions it was as high as 15:1. More typically, the ratio was between 5:1 and 10:1, and ranged down to 1.5:1 and less at the lowest current settings.

III. METHOD OF ANALYSIS

A. General Method

Our experimental methods differed from those of other workers in the field of pair spectrometry in one important respect: rather than take data at only one, or at most only a few magnetic field settings, we varied our magnetic field with small increments over a very wide range. This posed a rather unusual problem in data analysis. At each field setting, as many as 36 different energy channels (with the circular spectrometer) can be defined, depending upon the particular combination of counters producing the coincidence. Since we collected data at 16 different magnetic fields, this means that there are 576 different energy channels between minimum and maximum energies. The observed counting rate at each channel depends upon a number of factors: the "true" value of the spectrum at that energy, the geometry of the spectrometer, the magnetic field, the widths of the counters, the dimensions and thickness of the converter, the pair-production cross section at that energy, the loss due to vertical scattering of electrons in the converter out of the plane of the scintillators, and the degree of radiation straggling of electrons in the converter.

The problem of analysis is therefore twofold: The theory of the operation of a pair spectrometer must be thoroughly understood, along with the various nuclear processes which the electrons and gamma rays undergo; and secondly, these theories must be brought together to determine spectrometer efficiencies at each channel, and these channels consolidated, so that only a relatively small number of experimental points appear in the final spectrum.

In the early stages, the process of data analysis was performed entirely by hand. Data was manually recorded in the data book, and analysis consisted of making lengthy tables and calculations by hand. Errors were numerous and difficult to detect. The final spectrum reflected a number of compromises made in order to simplify data processing.

As our understanding of the spectrometer grew and our data became more precise, we recognized the need for some system of automatic data processing. A computer program was written to do what we had up to that point done by hand. This program has undergone a number of modifications and we now have a very high degree of confidence in its accuracy and effectiveness.

B. Description of the Data Analysis Program

The final version of our ESCHATON program for data analysis is designed for use on either an IBM 709 or 7090 computer. It performs the following functions:

(1) reads in data;
(2) makes the converter-out subtraction;
(3) normalizes all data using efficiencies as determined from spectrometer theory;
(4) corrects for vertical scattering losses and radiation straggling;
(5) groups data corresponding to similar gamma-ray energies into one experimental point;
(6) calculates its statistical error;
(7) makes the target out subtraction;
(8) joins data taken with the 180-deg and circular spectrometers;
(9) transforms the spectrum into center-of-mass coordinates;
(10) plots all results on a cathode ray tube;
(11) photographs then; and
(12) prints out numerical results.

Four preliminary calculations must be made: the scattering correction as a function of converter, magnetic field, and counter combinations; the pair-production cross section as a function of gamma-ray energy; the geometric efficiency of each spectrometer channel; and the radiation straggling correction. These were all computer-calculated, combined together and read out on magnetic tape. The formulas used for these calculations are derived in the appendices. Appendix A derives the basic theory of the spectrometer and shows how one arrives at the geometric efficiency. Appendix C gives the actual parameters used for the 180-deg and circular spectrometer. Appendix D indicates the method used to calculate the vertical scattering correction. The radiation straggling correction is described in Appendix B. Appendix E gives the pair-production formulas used.

ESCHATON begins by reading in all the efficiency and correction factors from the prepared tape. It then reads in the data on cards, sorting it according to magnet current and whether it is converter-in or-out, target-in or-out, and high (circular) or low (180-deg) spectrometer. Along with the number of coincidences in each channel, the cards also record the number

of dumps as measured by the SEM chamber (one dump corresponds to a certain total charge as integrated by the electrometer attached to the chamber). In order to simplify the later grouping or "binning" into a single experimental point and the calculation of experimental error, all corrections are applied to the number of dumps, rather than to the total number of counts. Thus, if channel A is inherently twice as efficient as channel B, the number of dumps in channel A is multiplied by 2 before combining the data with channel B, rather than dividing the counts by 2.

After the converter-out subtraction is made and the number of dumps adjusted by the various efficiency and correction factors, the data is combined into experimental points. This can be done in quite flexible fashion, according to the wishes of the experimenter. One reads in from cards a set of numbers corresponding to the energy of the end points of each "bin." The program then sorts the data into the proper bin, according to the energy of each channel, and averages all the data in each bin with the proper statistical weights. It also calculates an average energy for that bin, weighted by the amount of data included in each channel. With this feature, results can be obtained with experimental points as close together or as far apart as desired. One can obtain results with a small number of points and good statistics, or a large number of points with poorer statistics. One can also shift the end points of each bin and check for consistency in both the program and data.

The last phase of the program depends upon what kind of data has been read in. If there is both target-in and target-out data present, a subtraction is made and the resulting statistical error computed. If data from both the high and low spectrometers is present, points at the same energy are combined with the proper normalization and statistical weights. All the resulting spectra are then transformed into the two-proton c. m. system, the transforming factor depending upon the laboratory angle. These spectra are plotted on a cathode-ray tube and photographed. All results and certain intermediate steps are also read out in tabular form. The entire process of analysis and plotting takes approximately 2-1/2 minutes on the 709 for a typical set of data at one angle.

C. Normalizing Procedures

Ideally, if the spectrometers had been well plateaued, if their efficiencies were exactly those calculated by the spectrometer theory, and if the SEM monitor made precise measurements of all proton currents, all the observed gamma-ray spectra would have the proper normalization. In practice, however, this was not entirely true. Because of the problems associated with the loss of good vacuum in the SEM chamber mentioned in Sec. II-B-2 above, there was some uncertainty in the measurement of the proton currents during some sections of the run. Also, the spectrum measured with the circular spectrometer at a given angle did not exactly match the spectrum measured with the 180-deg spectrometer, in the region where the energies overlapped. The experimental points from the circular spectrometer were about 5% higher than those from the 180-deg spectrometer at each angle.

Because of these difficulties, the normalization of some sections of the data had to be adjusted. This was done by plotting the results of the analysis of various sections of data separately, then comparing the spectra point by point. If, on the average, the points from one section were uniformly lower than those from another section, then the data from the first section was multiplied by a constant factor before combining the two sections. The same procedure was followed in normalizing the spectra from the two spectrometers together. In almost all cases these adjustments were no larger than about 5%.

In Fig. 13 we show separately the spectra obtained from the 180-deg and circular spectrometers at 60 deg, after the normalizations had been adjusted. The observed spectra are essentially the same; the difference between any two points at the same energy is almost always less than the experimental error. This gave us confidence in the data-analyzing procedures. Physically, the two spectrometers are very different, and yet the spectra observed by the two instruments were essentially alike. The spectra matched equally well at the other two angles.

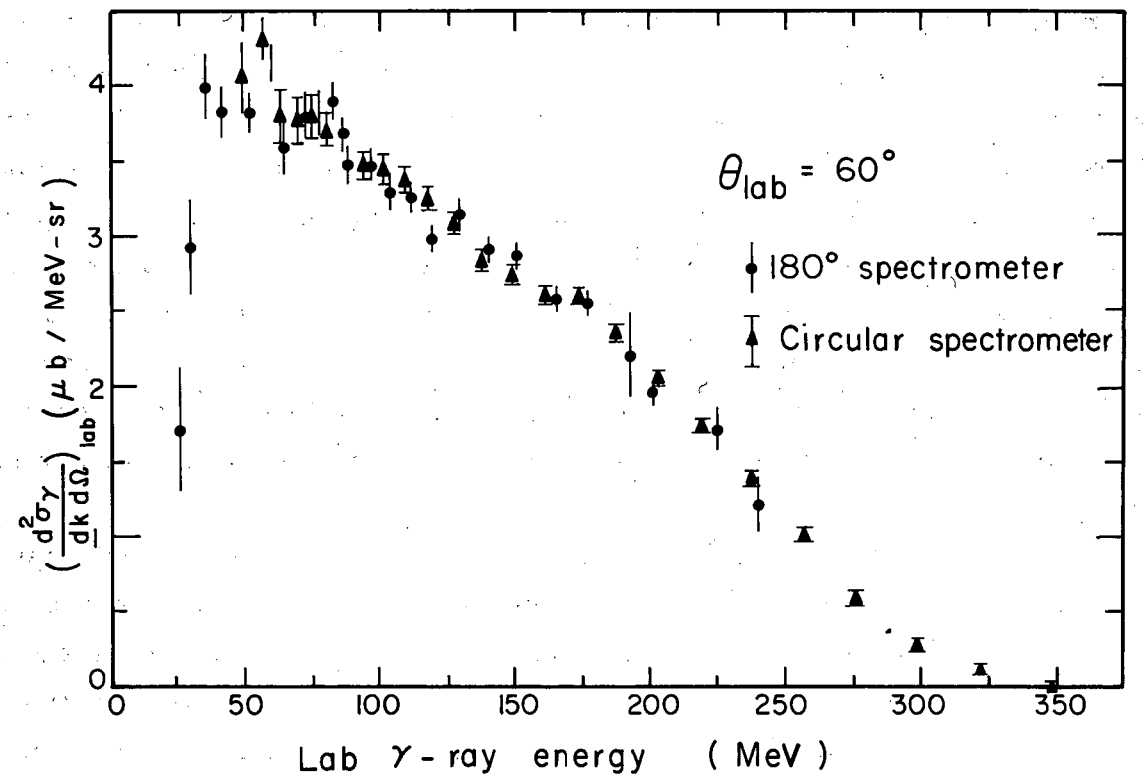

MUB-1082

Fig. 13. Spectra obtained with the circular spectrometer and the 180-deg spectrometer, plotted separately. Notice the close overlapping of points.

IV. RESULTS

A. Laboratory Gamma-Ray Spectra

The gamma-ray spectra observed at the three lab angles of 6, 32, and 60 deg are shown in Fig. 14. The high-energy cutoffs predicted by π^0 decay kinematics are at 540, 464, and 346 MeV, respectively. In each case the experimental cutoffs are almost exactly where predicted. Kinematic theory predicts a low-energy cutoff as well, at energies of 27, 23, and 17 MeV, respectively. Although the spectra did drop off sharply at the low-energy end, they never actually reached zero. We felt that this was due to a contamination of the low-energy part of the spectra from higher-energy gamma rays producing electron pairs somewhere in the channel. These electrons then underwent bremsstrahlung to produce gamma rays of lower energy. This is discussed at greater length in the section that describes the anticoincidence counter (II-C-2). Since the amount of contamination could not be accurately estimated, the parts of the spectra at the lowest energies were not used for subsequent analysis.

The errors shown are statistical errors only. The error on most points is less than 2%, except at the lowest energies. In addition, there are systematic errors of as much as 5% which would affect the total normalization of the spectra. These come primarily from uncertainties in the measurement of the proton current, due to problems encountered with the secondary emission monitor chamber.

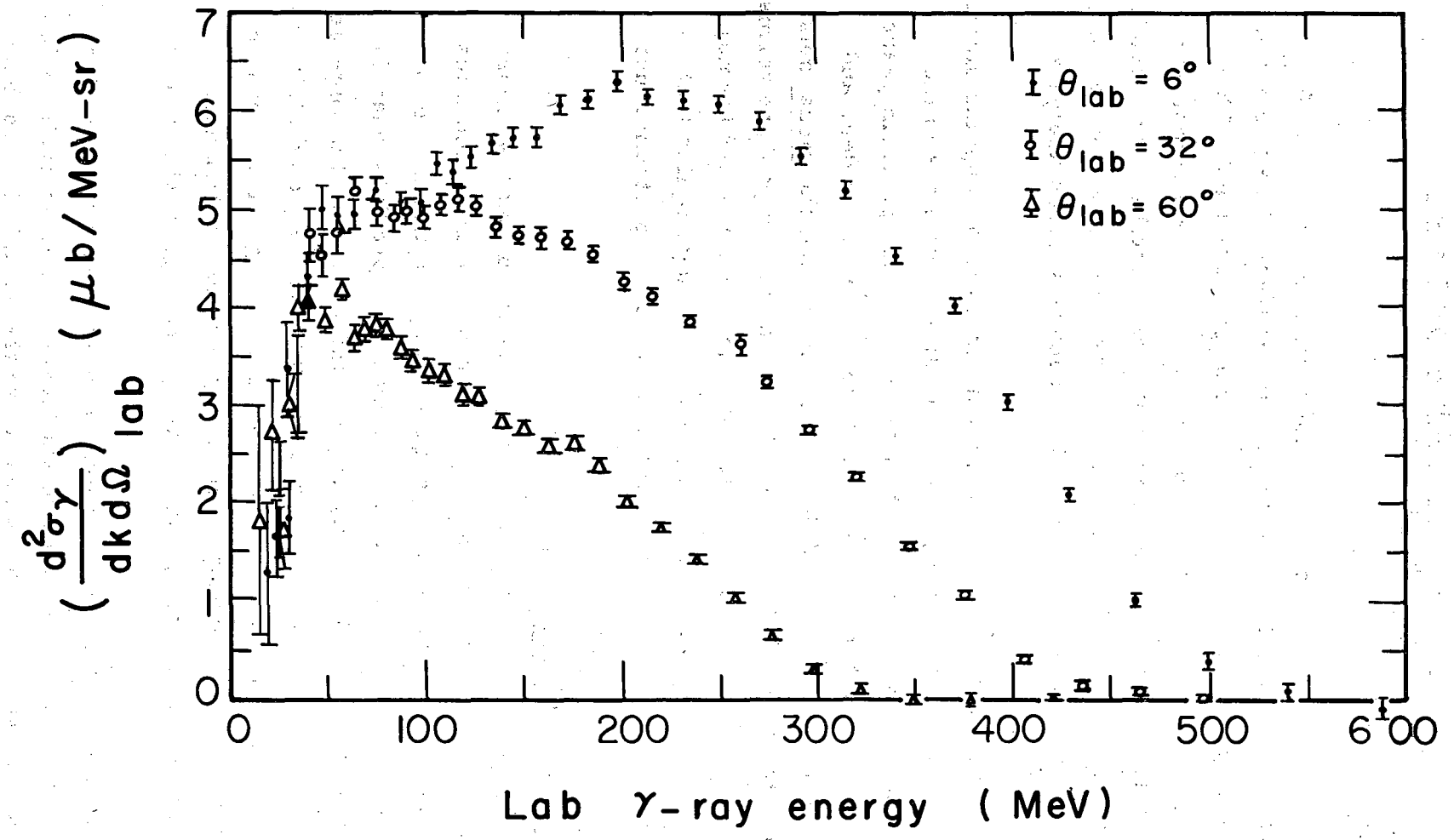

Fig. 14. The gamma-ray spectra as measured in the laboratory. The statistical error on most points is less than 2%.

B. Center-of-Mass Gamma-Ray and Pion Spectra and Total Cross Section

1. Gamma-ray spectra

In Figs. 15, 16, and 17 we show the same gamma-ray spectra after they have been transformed into the two-proton c.m. system. The predicted high-energy c.m. cutoffs are now all at the same energy: 301 MeV. The predicted low-energy cutoff is 15 MeV. The errors shown are a combination of two types: statistical errors, plus an estimated reproducibility error equal to 2% of the value of each point. This latter error was necessary in order to make the goodness-of-fit parameter $\chi^2/d = 1$ in the least-squares analysis described in the next section.

Examination of these spectra clearly indicate that the π^0 angular distribution cannot be purely isotropic, because of substantial differences in the gamma-ray spectra at the three angles. At 11 deg c.m., the spectrum peaks at about 110 MeV. There is a broad peak from 40 to 80 MeV at 55 deg, and the spectrum peaks around 40 MeV at 93 deg. This means that the pions must be peaked in the forward and back directions; that is, there are positive terms in the pion angular distribution proportional to $\cos^2\theta$ (or higher order terms). The fact that there is such a broad gamma-ray peak at 55 deg implies that very few of the pions are given off with low energy; the pion spectrum must be peaked at higher energies.

2. Method used to get pion distributions

To obtain any quantitative information on pion distributions, we must compare the results in detail with predicted spectra based on the kinematics of pion decay. If we assume any specific energy and angular distribution for the pions, the kinematic theory as developed in Appendix F predicts what the resulting gamma-ray spectra will be at any angle. Unfortunately, the reverse is not true. That is, it is not possible to directly determine the pion distributions in any analytic fashion from a knowledge of the gamma-ray spectra. Thus one is forced to begin with some assumptions concerning the pion distributions, then determine how well the predicted gamma-ray spectra agree with experiment.

Instead of choosing the pion distributions in rather haphazard fashion, we wrote a computer program that would make a least-squares analysis to determine the proper pion distributions for a best fit to the data. This was done as follows:

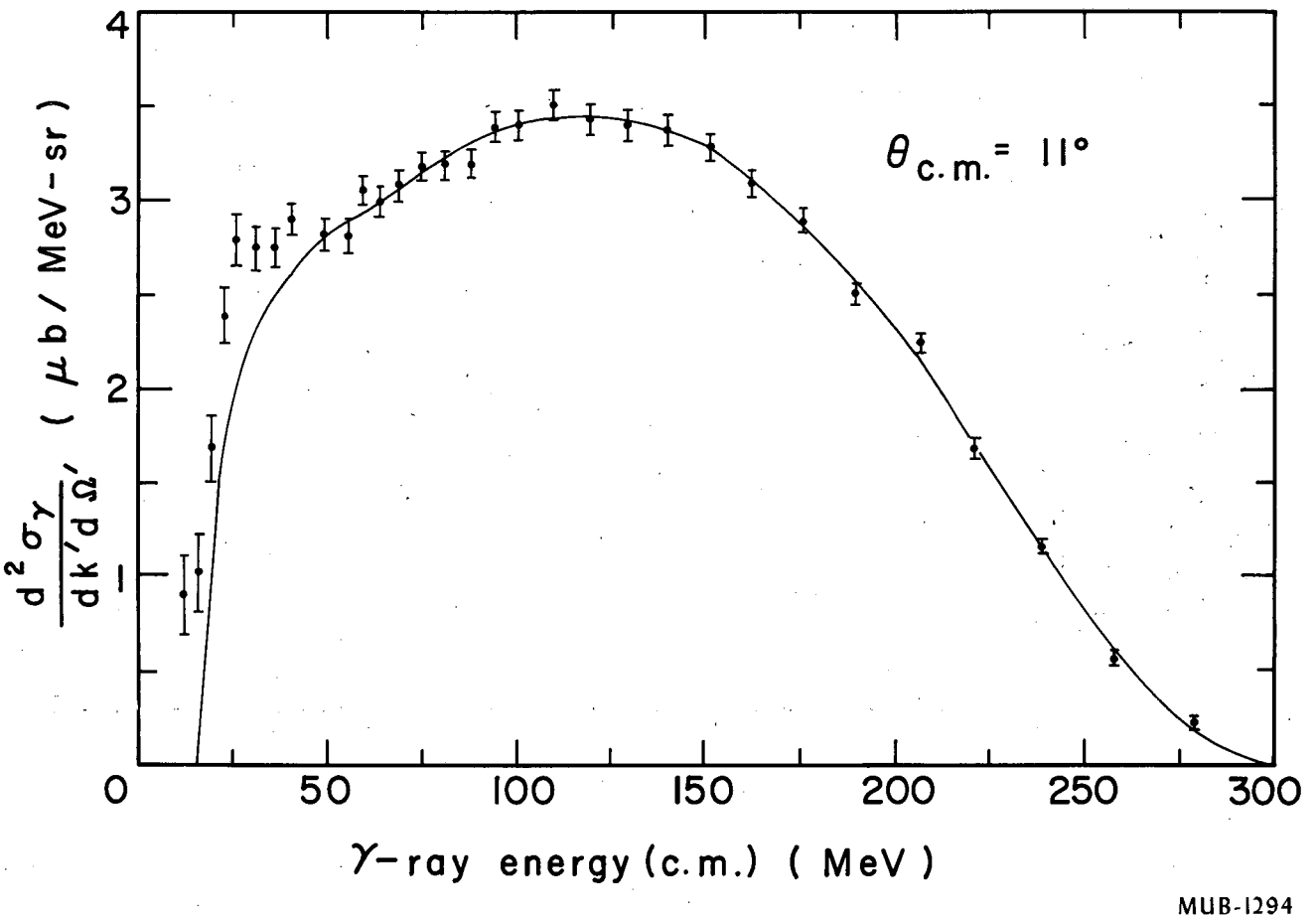

Fig. 15. The gamma-ray spectrum at 11 deg in the center of mass. The solid line shows the best fit to the data as determined by the least-squares program.

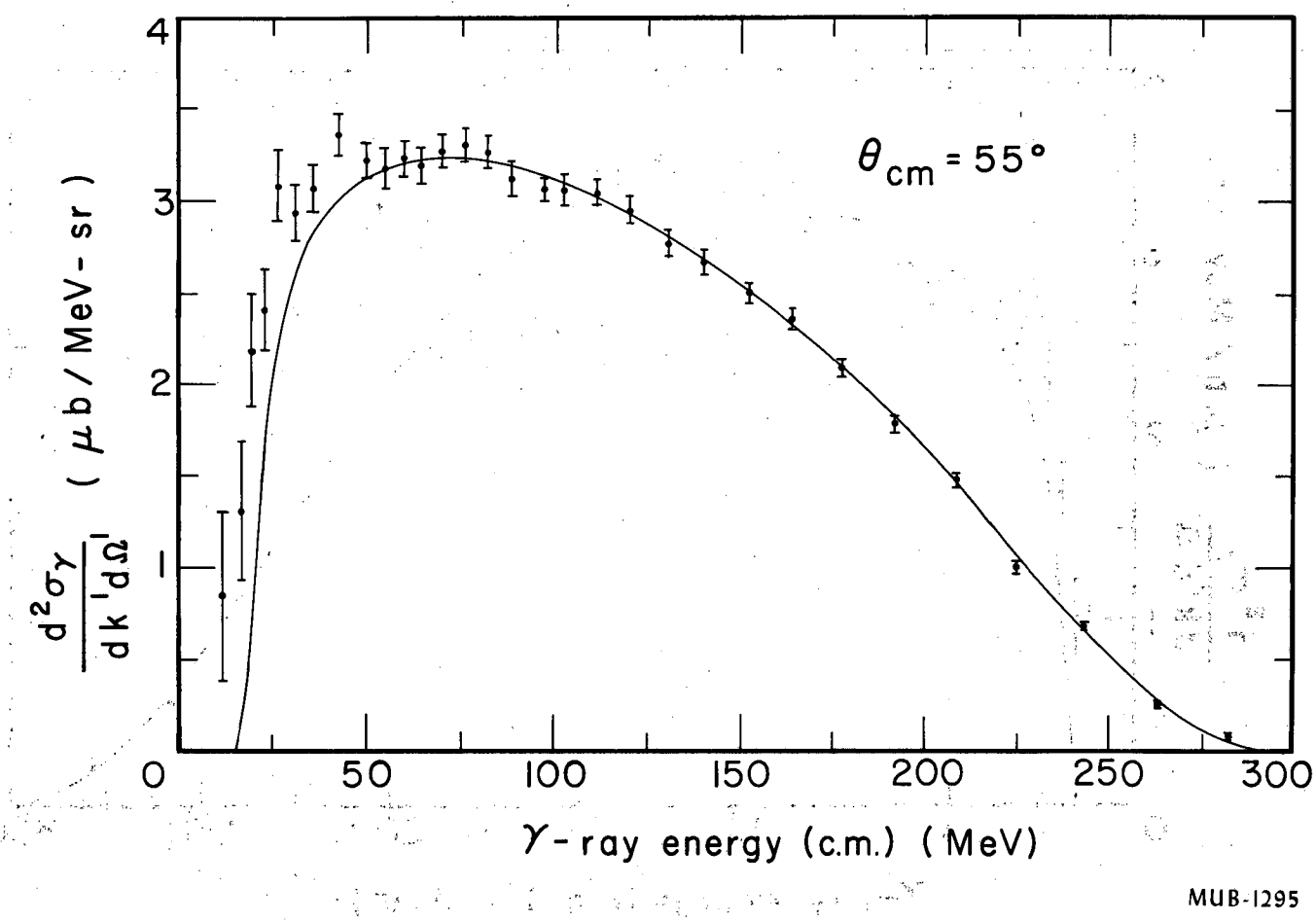

Fig. 16. The spectrum at 55 deg c. m. The solid line shows the best fit to the data.

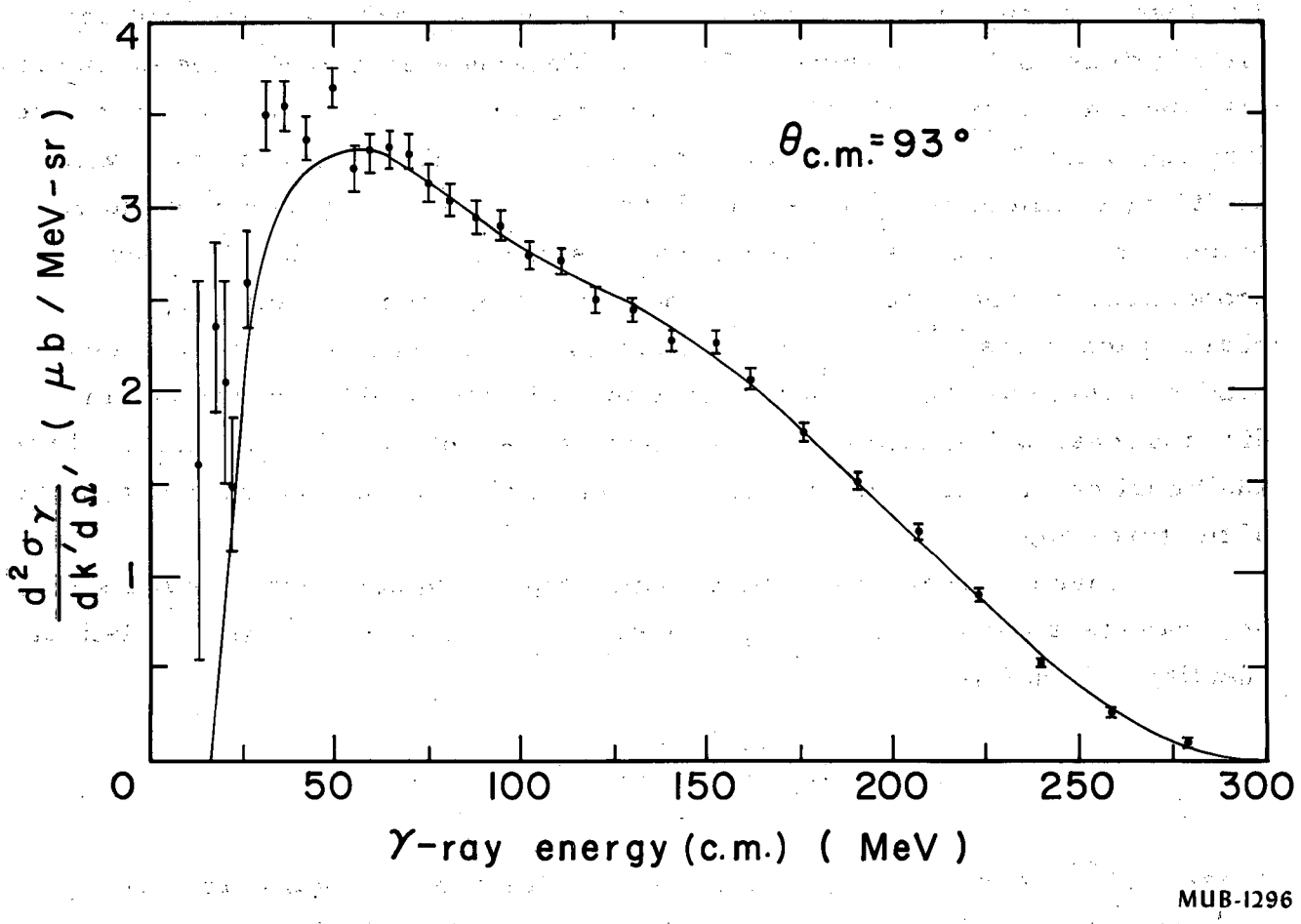

Fig. 17. The spectrum at 93 deg c. m. The solid line shows the best fit to the data.

A subprogram was written that would calculate gamma-ray spectra at each of the three angles at which our experiment was performed, starting with any arbitrary c.m. pion distributions. The angular distribution could be isotropic; proportional to $\cos^2\theta$ or $\cos^4\theta$, or any combination of these three. For that fraction of the pions produced isotropically, arbitrary momentum distributions could be assumed. This was done by assuming that the momentum distribution was proportional to the product of the three-body phase space term (see Appendix F for the exact form) and a polynomial in p (momentum) with arbitrary coefficients. This ensured that the momentum spectrum would go to zero at the end points. Thus one can assume momentum distributions proportional to phase space, phase space times p, times p^2, etc., up to phase space times p^8, or any combination of these. Similarly, those pions produced with $\cos^2\theta$ or $\cos^4\theta$ distribution could have arbitrary momentum distributions, which need not be the same as the isotropic distributions. Three additional parameters allowed one to assume arbitrary normalizations at each of the three angles.

A master program was then written that could start with a given set of parameters and calculate the goodness of fit as measured by the statistical quantity χ^2, defined by

$$\chi^2 = \sum_i \frac{\left(x_i^{exp} - x_i^{th}\right)^2}{\sigma_i^2},$$

where x_i^{exp} is the experimental point, σ_i the experimental error, and x_i^{th} the value of the spectrum at that energy predicted by kinematic theory, and the sum is over all the experimental points. The value of each arbitrary parameter is now varied in turn, to see whether one can improve the fit by reducing χ^2. The process of varying each parameter is continued until no variation in any of the parameters can make any further reduction in the value of χ^2. To ensure that this is indeed a unique solution, one uses many different starting points for the value of the parameters, and checks to see whether the ultimate solution is essentially the same. We found that the solution was indeed unique, so long as one did not allow too many of the parameters to vary.

3. Resulting pion distributions

The best fit to the gamma-ray spectra at each of the three c.m. angles as determined by the least-squares program is shown as a solid line in Figs. 15, 16, and 17. In making this fit, only points at energies greater than 50 MeV c.m. were used. It was felt that the spectra at energies lower than this were unreliable, because of the bremsstrahlung contamination mentioned above. Whenever experimental points at lower energies were included, the goodness of fit, as measured by the parameter χ^2, became much poorer.

The pion angular distribution for this solution is represented by

$$\frac{d\sigma_{\pi^0}}{d\Omega} = \frac{\sigma_{tot}}{4\pi} \left[0.834 + 0.099 \left(3 \cos^2\theta\right) + 0.067 \left(5 \cos^4\theta\right) \right] .$$

That is, approximately 83% of the pions are produced isotropically, 10% with $\cos^2\theta$ dependence, and 7% with $\cos^4\theta$ dependence.

We also attempted to find a solution where only isotropic and $\cos^2\theta$ terms were allowed. The resulting angular distribution is given by

$$\frac{d\sigma_{\pi^0}}{d\Omega} = \frac{\sigma_{tot}}{4\pi} \left[0.799 + 0.201 \left(3 \cos^2\theta\right) \right] .$$

Note that the fraction of pions with isotropic distribution is somewhat less for this solution (around 80%, instead of 83%). This is because the presence of a $\cos^4\theta$ term in the former case can produce a larger amount of anisotropy than the same amount of $\cos^2\theta$ production. To compensate for the lack of this term, therefore, the isotropic term must be reduced in the present solution. The shape of the angular distributions is almost the same, however, as can be seen in Fig. 18, where the angular distributions for the two solutions are plotted together.

The goodness of fit is somewhat poorer for this solution ($\chi^2/d = 1.0$ for this case, whereas $\chi^2/d = 1.2$ when $\cos^4\theta$ terms are allowed; d is the number of degrees of freedom). However, a sufficiently good fit is obtained so that it is not possible to say with certainty that $\cos^4\theta$ production is necessary to explain the results. We can say definitely that the production is approximately 80% isotropic. We cannot define with any precision the nature of the anisotropic term. For this reason, we cannot make any reasonable assignment of error to the individual terms in the angular distribution.

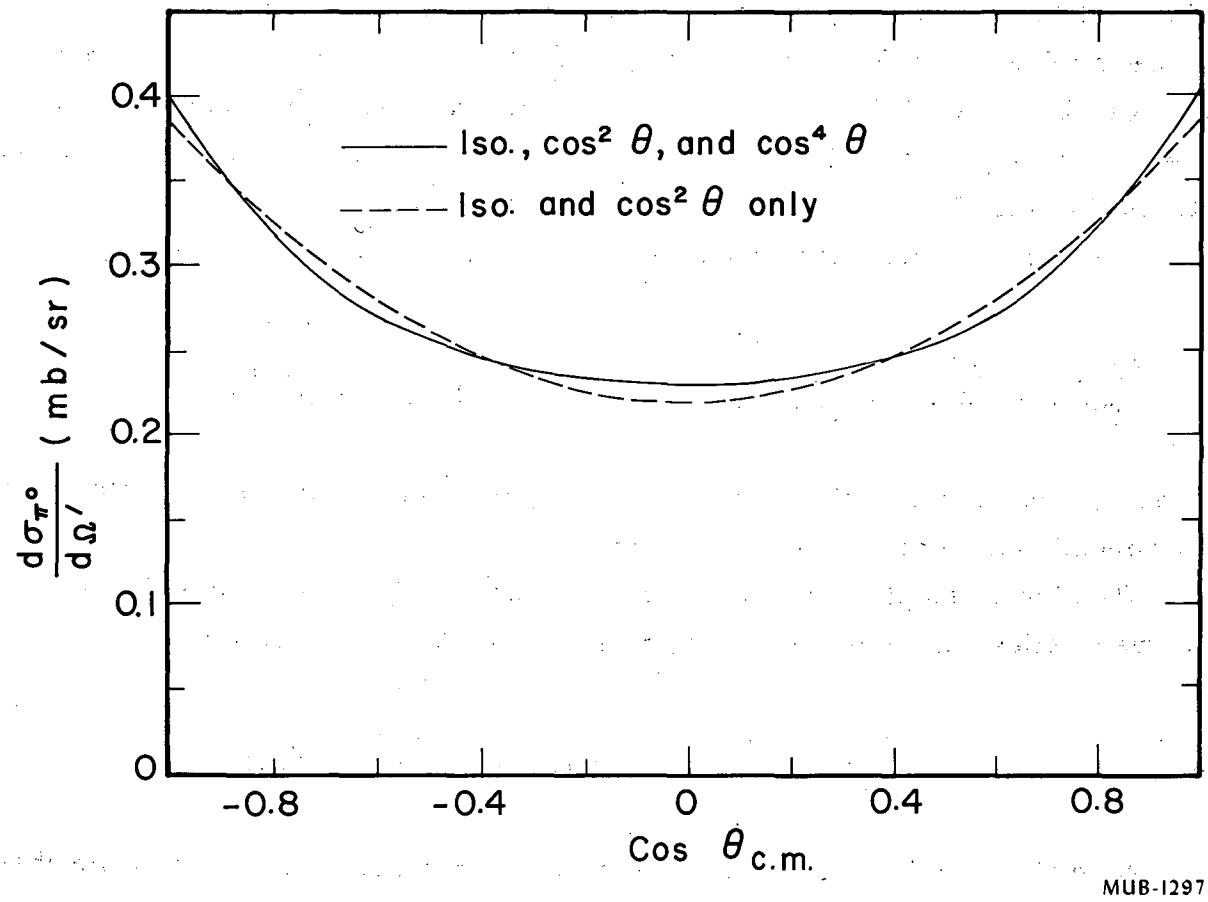

Fig. 18. π^0 angular distributions in the two-proton c. m. system. The solid line shows the distribution when terms through $\cos^4\theta_{c.m.}$ are included. The dashed line shows the distribution when only isotropic and $\cos^2\theta_{c.m.}$ terms are permitted.

The pion momentum distributions at the c. m. angles of 0, 45, and 90 deg are shown in Fig. 19, along with the (isotropic) spectrum one would expect if the differential cross section were proportional to the available phase space. The independent variable is the pion momentum η in multiples of μc, where μ is the π^0 rest mass. The solution containing $\cos^4\theta$ terms is used here. The curves for the second solution are almost identical to those shown in Fig. 19.

As might be expected, the pions emitted at 0 deg are peaked at higher values of momentum than those emitted at 90 deg. At all three angles, the average momentum is somewhat less than that predicted from phase space calculations. In fact, the distribution centered around lower values of momentum is just what one would expect from an analysis based on the isobar model of pion production. This point is discussed further in the Summary and Conclusions section.

4. Total cross section

The total cross section for the reaction $p + p \rightarrow p + p + \pi^0$ can be obtained from the results of the least-squares program. If the gamma-ray spectra used as the data input are properly normalized, then the normalizing parameters selected by the least-squares program are related to the total cross section. In Part 3 of Appendix F we relate all the factors that must be used to calculate the total cross section. The result is

$$\sigma_{\text{total}} (p + p \rightarrow p + p + \pi^0) = 3.46 \pm 0.25 \text{ mb.}$$

The error is primarily due to uncertainty in the measurement of the absolute proton flux striking the hydrogen target. This result can also be obtained by integrating the gamma-ray c. m. spectrum at the "isotropic" angle, $\theta_{\text{c.m.}} = 55$ deg, over gamma-ray energy, and multiplying by $4\pi/2$ (since each π^0 produces two gamma rays). This, of course, assumes no terms higher than $\cos^2\theta$ in the pion angular distributions.

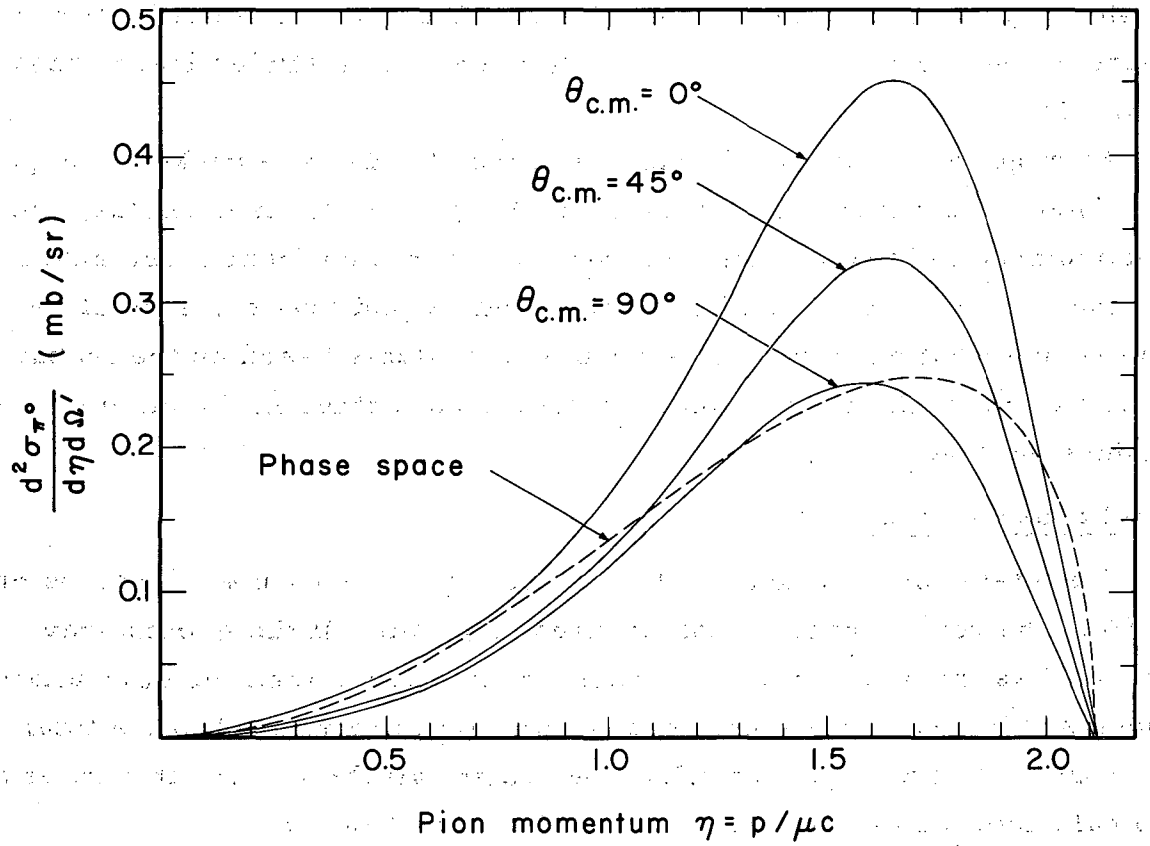

Fig. 19. The π^0 momentum distributions at c.m. angles of 0, 45, and 90 deg. The dashed line is the distribution calculated from phase space.

V. SUMMARY AND CONCLUSIONS

We now summarize the results of this experiment and attempt to draw some conclusions. We have measured the gamma-ray spectra from a hydrogen target bombarded by 735-MeV protons at three laboratory angles. The resulting spectra are shown in Fig. 14 and the equivalent spectra in the two-proton c. m. system are shown in Figs. 15-17. The spectra exhibit the general characteristics expected from the decay of neutral pions produced with a total cross section of 3.46 ± 0.25 mb. The spectra were compared with the predicted spectra based on pion-decay kinematic theory, using a least-squares computer program, and pion angular and momentum distributions were determined. The angular distribution is given by

$$\frac{d\sigma_{\pi^0}}{d\Omega} = \frac{\sigma_{tot}}{4\pi} \left[0.834 + 0.099 \left(3 \cos^2\theta\right) + 0.067 \left(5 \cos^4\theta\right) \right]$$

and is shown in Fig. 18; and the momentum distributions, along with the distribution calculated on the basis of available phase space, are shown in Fig. 19.

It is perhaps somewhat surprising that the pion angular distribution is so nearly isotropic. Over 80% of the pions are produced with isotropic distribution. Most nuclear processes become highly anisotropic as the energy increases. Partial-wave analysis based on classical impact parameter theory indicate that high-order angular distribution terms could very well be important. However, if the production proceeds primarily through the intermediate creation of a nuclear isobar, which subsequently decays into a proton and a π^0 meson, one expects the reaction to be mostly isotropic. After creation of the isobar, very little kinetic energy remains. In our case, approximately 40 MeV is available to the proton and an isobar of mass 1230 MeV. The isobar would therefore be produced primarily in an s state, with isotropic production. The pions would therefore also be mostly isotropic. The presence of small higher-order terms would indicate some p-wave production of the isobar.

We may compare our pion angular distributions with those of Dunaitsev and Prokoshkin.[23] They measured the value of the parameter b at energies of from 400 to 665 MeV, where b is the constant in the angular distribution given by

$$\frac{d\sigma_{\pi^0}}{d\Omega} \propto \frac{1}{3} + b \cos^2\theta_{c.m.} .$$

They find b to be statistically zero except at 665 MeV, where $b = 0.10 \pm 0.03$ (see Fig. 20). In other words, the reaction is almost completely isotropic. In order to make a direct comparison, we must use our solution in which the $\cos^4\theta$ term was omitted. In this case $b = 0.25 \pm 0.04$. (The error quoted here was estimated by noting the approximate sensitivity of χ^2 to b.) Thus it would appear that the anisotropic term is increasing rapidly in the energy region from 665 to 735 MeV.

Additional evidence for pion production proceeding primarily through the creation of an isobar comes from the observed pion momentum distributions. Here there is a significant departure from phase space predictions, with the observed pions peaked at somewhat lower values of momentum (see Fig. 19). In fact, the observed distributions are very similar to those which would be expected if the pions came from the decay of a nuclear isobar of energy 1.23 BeV.

In summary, we find that the gamma rays observed from a hydrogen target bombarded with 735-MeV protons appear to arise entirely from the decay of neutral pions produced within the target. This hypothesis explains all of the characteristics of the observed spectra, and a detailed analysis of the spectra provides quite reasonable results for pion production cross sections and angular and energy distributions. We find no evidence for gamma rays produced from any source other than neutral pion decay.

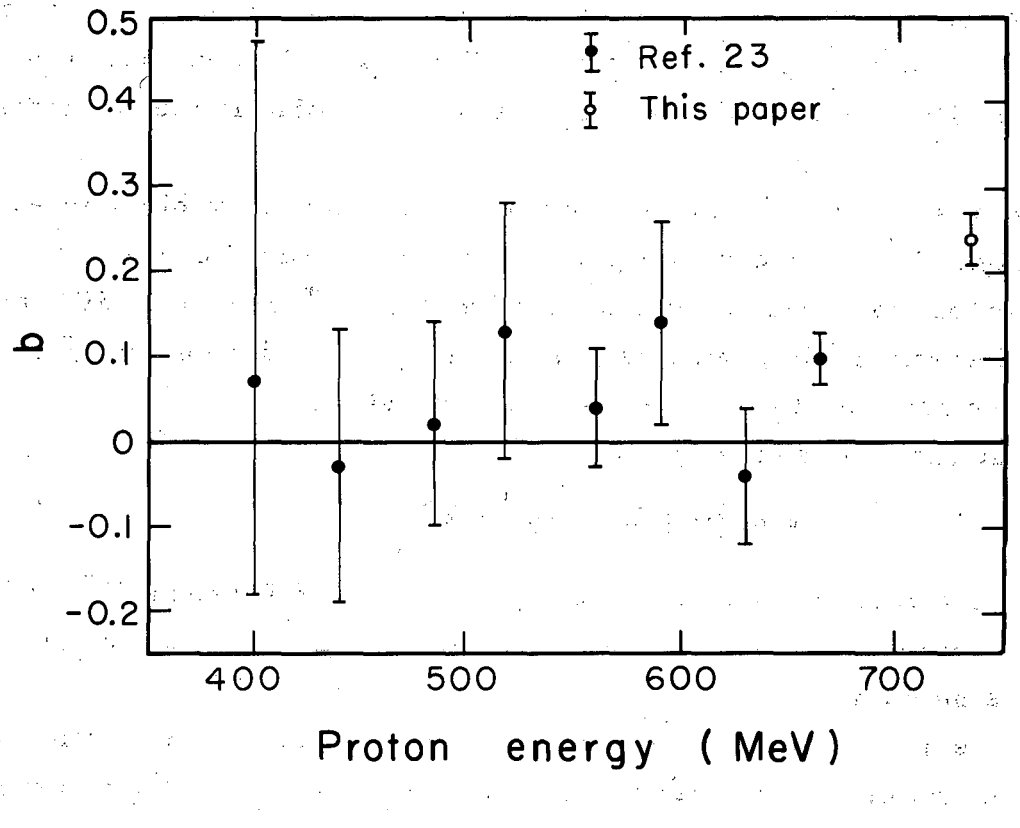

Fig. 20. Values of the coefficient b in the expansion

$$\frac{d\sigma_{\pi^0}}{d\Omega} \propto \left(\frac{1}{3} + b \cos^2\theta_{c.m.}\right) .$$

APPENDICES

A. Theory of the Pair Spectrometer

Let us assume we have a beam of gamma rays whose energies are such that the number of gammas per second striking a converter with energies between k and $k + dk$ is given by $F(k)dk$.

We place a pair of counters in a magnetic field with a given geometric configuration and ask the basic question: How many electron-positron pairs per second will be observed by the counters, i.e., what is the coincidence rate R?

We assume the converter is made of material of atomic number Z, atomic weight A, and thickness t g/cm^2. The differential cross section for the creation of a positron of total energy between E^+ and $E^+ + dE^+$ and a negative electron E^- by a gamma ray of energy k is denoted by $\underline{\phi}(k, E^+)dE^+$. The form we have used for $\underline{\phi}$ is given in Appendix E.

Thus the double differential

$$F(k)\,\underline{\phi}(k, E^+)\,\frac{t\,N_0}{A}\,dE^+dk$$

represents the rate of creation of positrons of energy between E^+ and $E^+ + dE^+$ from gamma rays of energy between k and $k + dk$. N_0 is Avogadro's number.

Now suppose that the positron counter is placed in a magnetic field H such that the minimum and maximum radii of curvature that the positron may have and still be detected by the counter are given by r^+_{min} and r^+_{max}. The average radius of curvature is r^+_{av}. The corresponding radii for the electron counter are r^-_{min}, r^-_{max}, and r^-_{av}. For the purpose of determining these radii, we assume the electrons come from the center of the converter. The fact that the converter has finite width will affect the resolution function, but not the efficiency factors which we are at present determining.

We denote corresponding energies as follows:

$$E^+_{av} = H\,r^+_{av},$$

$$E^+_{max} = H\,r^+_{max}, \text{ etc.},$$

and

$$k_{av} = E^+_{av} + E^-_{av} = H\,(r^+_{av} + r^-_{av}).$$

Note that these equations hold only if the electrons are highly relativistic, as they are in our application. Note also that we have eliminated a constant factor to save confusion (actually, $E^+ = 300\ H\ r^+$ if r^+ is in cm, H is in gauss, and E^+ is in electron volts).

Thus the positron counter will detect all positrons with energies between E^+_{max} and E^+_{min}, with average energy E^+_{av}, and this is likewise true for the electron counter.

To determine the coincidence rate, we must now perform a double integration, one over the range of gamma-ray energy k and the second over the range of positron energies E^+ for a given k. To aid us in this integration, we define a step function $S(k, E^+)$, which is equal to unity if k and E^+ are such that both the electron and positron are detected, and equal to zero otherwise.

We refer to Fig. 21 to aid us in our determination of S. Positron energies are plotted along the abscissa, and electron energies along the ordinate. Lines of constant gamma-ray energies are diagonals as shown. The rectangle corresponds to those values of E^+ and E^- for which the step function S is unity, i.e., a coincidence will be observed. S is zero outside the rectangle.

We may now begin to define S mathematically:

$$S(k, E^+) = 0 \quad \text{if} \quad k < H\,(r^+_{min} + r^-_{min}),$$

or if

$$k > H\,(r^+_{max} + r^-_{max}).$$

For k lying between these two values, S depends upon the value of E^+. We assume, as in the diagram, that the rectangle is taller than it is wide, so that

$$(r^-_{max} - r^-_{min}) > (r^+_{max} - r^+_{min}).$$

We now define three regions:

Region I: $H(r^+_{min} + r^-_{min}) < k < H\,(r^+_{max} + r^-_{min})$.

Here we have $S(k, E^+) = 1$ if $H\,r^+_{min} < E^+ < (k - H\,r^-_{min})$;

otherwise, $S(k, E^+) = 0$.

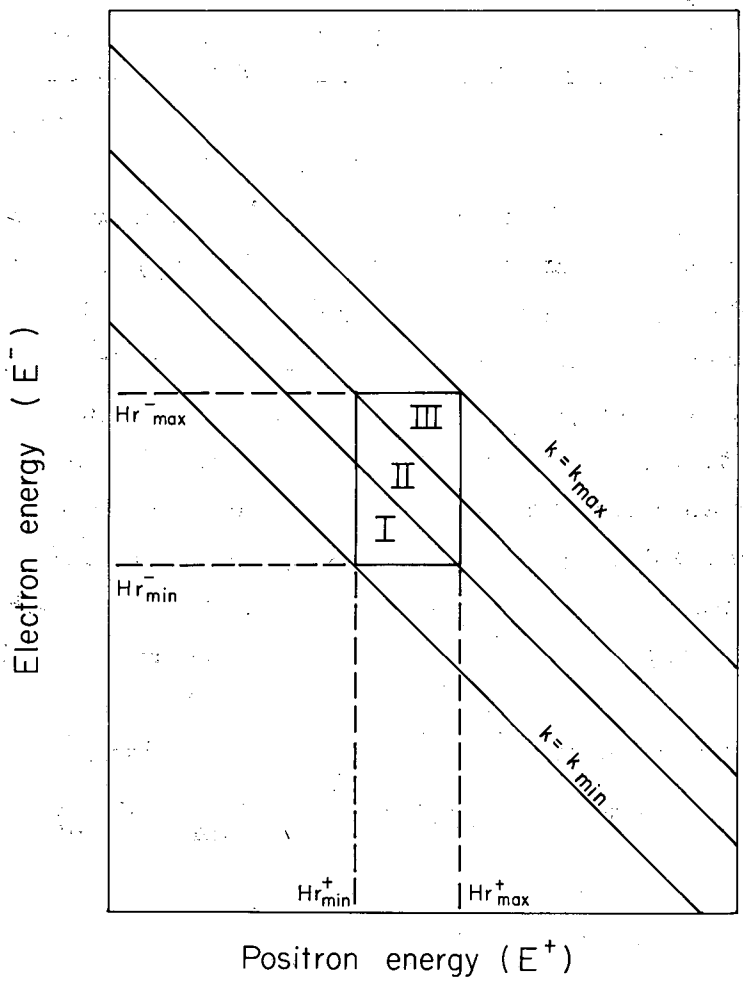

Fig. 21. Diagram used in performing integration to calculate spectrometer efficiency. Lines of constant γ-ray energy are diagonals.

Region II: $H\,(r^{+}_{max} + r^{-}_{min}) < k < H\,(r^{+}_{min} + r^{-}_{max})$.

Here we have $S(k, E^{+}) = 1$ if $H\,r^{+}_{min} < E^{+} < H\,r^{+}_{max}$;

otherwise, $S(k, E^{+}) = 0$.

Region III: $H\,(r^{+}_{min} + r^{-}_{max}) < k < H\,(r^{+}_{max} + r^{-}_{max})$.

Here we have $S(k, E^{+}) = 1$, $(k - H\,r^{-}_{max}) < E^{+} < H\,r^{+}_{max}$;

otherwise, $S(k, E^{+}) = 0$.

Having thus defined the function $S(k, E^{+})$, we may now write the coincidence rate R in terms of the double integral as follows:

$$R = \frac{t\,N_0}{A} \int_{k=0}^{k_{max}} F(k) \left[\int_{E^{+}=0}^{k} \underline{\phi}(k, E^{+})\, S(k, E^{+})\, dE^{+} \right] dk .$$

The solution of this integral is straightforward. The integral over k is divided into three parts, corresponding to the three regions as defined above. Within each region, the definition of $S(k, E^{+})$ is used to define the limits of integration over E^{+} and k. We must make two approximations:

(1) We assume that the spectrum $F(k)$ is not rapidly changing over the region of integration. We may therefore substitute its average value, equal to the energy at the midpoints of the counters, and take the function $F(k_{av})$ outside the integral.

(2) We assume that the differential pair production cross section $\underline{\phi}(k, E^{+})$ is not rapidly varying over the region of integration. Its average value is also substituted, and the function brought out in front of the integral.

The final result of the double integration is:

$$R = \frac{t\,N_0}{A}\, F(k_{av})\, \underline{\phi}(k_{av},\, E^{+}_{av})\, \Delta E^{+}\, \Delta E^{-} ,$$

where

$$\Delta E^{+} = H\,\Delta r^{+} = H\,(r^{+}_{max} - r^{+}_{min}) ,$$

and

$$\Delta E^{-} = H\,\Delta r^{-} = H\,(r^{-}_{max} - r^{-}_{min}) .$$

Since the total pair-production cross section varies only slowly with gamma-ray energy, whereas the differential cross section goes approximately as $1/k$, the cross section usually plotted in the literature is $k\underline{\phi}$. Using the fact

that $k = H(r^+ + r^-)$, we may rewrite the above as

$$R = \frac{t N_0}{A} F(k) \left[k \bar{\phi}(k, E^+) \right] \left[\frac{H \Delta r^+ \Delta r^-}{r^+ + r^-} \right] .$$

Note that Δr^+ and Δr^- are not the physical widths of the detectors. They refer only to the range of electron radii that can be detected. This range is a function both of the detector widths and their positions in the spectrometer. See Appendix C for the values of Δr and r.

In this final form, we drop the subscript denoting averages, and assume that values corresponding to the center of the detectors will be used.

We emphasize again that in actual calculations a constant factor must be included so that the final bracket will have the dimensions of energy.

Two important factors have been omitted from this analysis. First, we have not taken into consideration losses in counting rate due to vertical scattering of electrons out of the plane of the counter. This is discussed in Appendix D. Secondly, we have not considered the change in the spectrum due to radiation straggling in the converter. This correction is discussed in Appendix B.

The final bracket is the geometric efficiency of the spectrometer. In our data analysis, this factor was calculated for each counter combination at each magnetic field and multiplied by the corresponding factors for pair production and scattering loss. The resulting table was stored on magnetic tape and read in at the beginning of the ESCHATON program.

B. Resolving Power of the Spectrometer

The resolving power of a spectrometer depends on several factors. The two most important are the geometric resolving power due to finite detector widths and the radiation straggling of electrons in the converter. Other factors are horizontal scattering of electrons, effects due to finite widths of the converter, and pair production at finite angles with respect to the incoming beam of gamma rays. Each of these factors will be discussed below. Only the first two were used to correct the observed spectra.

1. Geometric Resolving Power

The geometric resolving power can be obtained by performing only one of the two integrations in the expression for the spectrometer efficiency derived in Appendix A. Recalling the definition of the step function $S(k, E^+)$, and neglecting constant factors, we may write the geometric resolution function $F_{geom}(k)$ as

$$F_{geom}(k) = \int_{E^+=0}^{k} S(k, E^+)dE^+ .$$

As before, we use Fig. 21 to redefine the integral in three different regions of k, using the properties of the step function to establish the limits of integration. After the integration is performed, the following result is obtained (as before, we assume that $\Delta r^- \gtrsim \Delta r^+$):

Region I: $H(r^+_{min} + r^-_{min}) < k < H(r^+_{max} + r^-_{min})$;

$$F_{geom}(k) = k - H(r^+_{min} + r^-_{min});$$

Region II: $H(r^+_{max} + r^-_{min}) < k < H(r^+_{min} + r^-_{max})$,

$$F_{geom}(k) = H(r^+_{max} - r^+_{min}) = H\,\Delta r^+ ;$$

Region III: $H(r^+_{min} + r^-_{max}) < k < H(r^+_{max} + r^-_{max})$,

$$F_{geom}(k) = H(r^+_{max} + r^-_{max}) - k .$$

A constant factor must multiply the HXr products in order to give them the correct energy units.

This resolution function is plotted in Fig. 22. We may note several characteristics:

(a) In the general case, the resolution function takes the form of a trapezoid. In the special case where $\Delta r^+ = \Delta r^-$, this reduces to a triangular function. This, in fact, was the case with our 180-deg spectrometer, but not with the circular spectrometer, except for symmetric counter pairs.

(b) The total width of the resolution function is H $(\Delta r^+ + \Delta r^-)$. Expressed as a fraction of the total gamma-ray energy, this reduces to

$$\text{Fractional resolution} = \frac{\Delta r^+ + \Delta r^-}{r^+ + r^-} \quad .$$

We may use the parameters given in Appendix C to determine the percentage resolution for each spectrometer:

(1) For the 180-deg spectrometer ($\Delta r^+ = \Delta r^- = 0.5$ in.),

$$\text{Fractional resolution} = \frac{1 \text{ in.}}{r^+ + r^-} \quad ;$$

(2) For the circular spectrometer $\left(\Delta r^\pm = \frac{1.5\, r^\pm}{15.875}\right)$:

$$\text{Fractional resolution} = \frac{1.5}{15.875} = 0.096.$$

Thus resolutions for the 180-deg spectrometer ranged from 7% to 17%, depending upon the counter combination. The circular spectrometer had a uniform resolution of about 10%. The half-width, of course, would be half of these numbers.

2. Radiation Straggling

After an electron-positron pair has been produced by a gamma ray in the converter, the electrons and positrons can undergo radiative collisions or bremsstrahlung during their passage through the remainder of the converter. These processes cause them to lose a certain fraction of their initial energy. For electron energies above 10 MeV, this energy loss in Ta (z = 73) is large compared to the loss from inelastic atomic collisions, and therefore the latter can be ignored. At these higher energies, the average radiative loss is proportional to the remaining thickness of converter and to the initial electron energy. Specifically,

$$-\left(\frac{dE}{dx}\right)_{rad} \approx \frac{E}{X_0} \quad ,$$

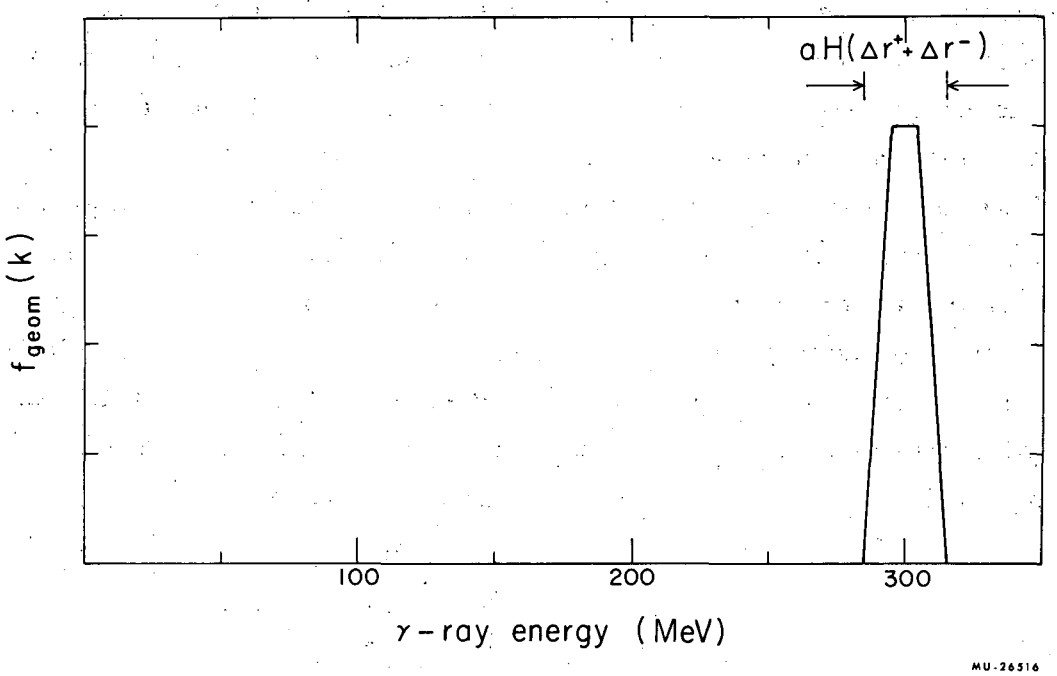

Fig. 22. Plot of the geometric resolution function. The shape is either trapezoidal or triangular, depending upon the specific geometry.

where X_0 is 1 radiation length of the converter material and E is the electron or positron energy. For tantalum, 1 radiation length is 6.4 g/cm^2. For the most part we used a 10-mil converter 0.41 g/cm^2 thick in the circular spectromter, and a 4-mil converter 0.17 g/cm^2 thick in the 180-deg spectrometer. Since on the average the electrons and positrons pass through only one half of the converter, the average energy loss was therefore about 3% for the circular spectrometer and about 1.3% for the 180-deg spectrometer. As a first approximation, therefore, we may correct for radiation losses by shifting the energy scale of the observed gamma-ray spectra upward by these percentages.

However, there is a large amount of straggling in the energy loss. In particular, the most probable energy loss is zero, yet some of the electrons will lose almost all their energy. The exact calculation of the electron distribution cannot be done analytically. Bethe and Heitler[34] use a simplified expression for the radiation probability and show that the probability that an electron of initial energy E_0 has energy between E and E + dE after traversing a thickness of t radiation lengths is given by

$$w(E_0, E, t)\, dE = \frac{dE}{E_0} \frac{\left(\ln \frac{E_0}{E}\right)^{\frac{t}{\ln 2} - 1}}{\Gamma\left(\frac{t}{\ln 2}\right)} .$$

For thin converters $(t << 1)$,

$$\Gamma\left(\frac{t}{\ln 2}\right) \approx \frac{\ln 2}{t} ,$$

and we have

$$w(E_0, E, t)\, dE = \frac{dE}{E_0} \frac{t}{\ln 2} \frac{1}{\left(\ln \frac{E_0}{E}\right)^{1 - \frac{t}{\ln 2}}} .$$

Since pair production can occur anywhere in the converter, an integral must be taken through the converter. Ryan[35] has developed an IBM program entitled CANIS MAJOR that we used in calculating our radiation straggling correction. This program uses as input a given converter thickness and electron and positron energy, then uses more accurate equations for the radiation probability to determine the electron energy spectrum after passing through a certain fraction of the converter. An integration through the converter

is performed, and the electron and positron distributions are folded together to determine what the observed gamma spectrum would be with a monoenergetic incident gamma beam and a given pair fragment splitting. A typical result for a 300-MeV gamma beam and 10-mil tantalum converter is shown in Fig. 23.

In making corrections to the experimental data the geometric resolution fraction was folded with the radiation straggling function at a number of gamma-ray energies and the resulting function folded into several typical theoretical spectra. (The "fold" h(x) of the functions f(y) and g(y) is defined as $h(x) = \int f(y)\, g(x-y)\, dy$.) The amount by which the theoretical spectra were changed then represented the correction that must be applied to the raw experimental data. The IBM 7090 was used to perform the folding operations and determine the corrections.

3. Other Factors

Several other factors can broaden the total resolution function, but in our case these were all small in comparison with the two effects already discussed. We will, however, make brief mention of them.

a. Horizontal scattering of electrons. Electrons and positrons can be scattered horizontally as well as vertically by the converter (see Appendix D for discussion of the latter effect). Horizontal scattering cannot affect the spectrometer efficiency, since on the average as many electrons are scattered into a given detector as are scattered out. However, the resolution function will be somewhat broadened. To first order, this effect is zero for a 180-deg spectrometer, due to the refocussing of rays with the same radius of curvature at the 180-deg point. With the circular spectrometer, the broadening effect due to horizontal scattering is largest at low energies. The effect becomes negligible at the higher energies at which this spectrometer was normally operated. A 70-MeV electron passing through half of a 10-mil tantalum converter will have a projected rms horizontal scattering angle of around two degrees. The resulting deflection at the detector is something less than half the width of a typical scintillator. The effect must therefore be smaller than that due to the finite widths of the detector, which is discussed in the first section of this appendix. The degree of broadening is inversely proportional to the energy.

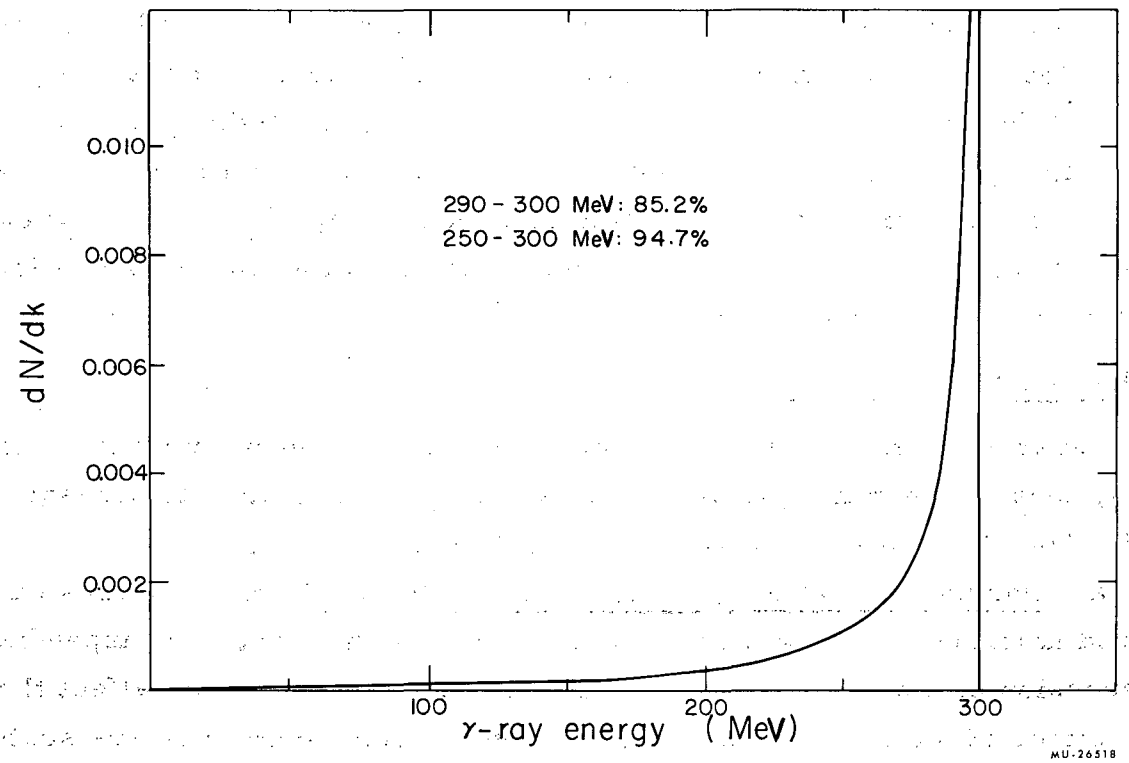

Fig. 23. Radiation straggling for a 300-MeV gamma ray and a 10-mil converter. The most probable energy loss is zero.

b. Angular distribution of pair electrons. The electrons are produced in the conversion process at a finite angle with respect to the incoming gamma ray. This angle is of the order $\theta_0 = mc^2/E$, where E is the total electron or positron energy. Since the mean-square projected scattering angle after traversing t radiation lengths of converter is given by

$$\theta_{\text{rms}}^{\text{scattering}} = \frac{14}{E}\sqrt{t},$$

where E is measured in MeV, we find that the ratio of these two angles is

$$\frac{\theta_0}{\theta_{\text{rms}}^{\text{scattering}}} \approx \frac{1}{30\sqrt{t}},$$

independent of energy. Since our thickest converter was 6% of a radiation length, and the electrons pass through half the converter on the average, this ratio is approximately 0.2. Therefore effects due to the angular distribution of pair electrons are small compared with effects due to electron scattering.

c. Finite converter widths. The spectrum measured by the circular spectrometer is broadened, because the converter is not infinitely narrow. There is no broadening with the 180-deg spectrometer, because if a gamma ray converts over to one side of the converter, the apparent change in energy of the electron is compensated exactly by a corresponding change in the apparent energy of the positron. Thus a 180-deg spectrometer may have a converter as wide as may be desired, without losing resolution.

Such was not the case with our circular spectrometer. In our particular geometry, no error will occur if the event is detected by a pair of symmetrically-placed counters. In the general case, one can show that to first order the fractional error in the observed gamma-ray energy due to a conversion at a distance δ from the center of the converter is given by

$$\frac{\Delta k}{k} = \frac{\delta\,(r^+ - r^-)}{2R^2},$$

where r^+ and r^- are the positron and electron radii of curvature, and R is the radius of the circle on which the detectors lie. Since $R = 15.9$ in., $\delta_{\text{max}} = 1$ in. (our converter was 2 in. wide), and $r^+ - r^- = 17.25$ in. for the most widely separated counter pairs, the maximum error in measurement of gamma-ray energies is 3.4%. In the majority of cases the error is less than 1%.

C. Spectrometer Parameters

In this section we list in tabular form the various parameters associated with the two spectrometers.

(1) Radii of curvature for electrons entering midpoint of detector.

Counter Number	180-deg Spectrometer (in.)	Circular Spectrometer (in.)
1	3	5.6
2	4	7.3
3	5	9.1
4	6	11.1
5	7	13.3
6	8	15.9
7		19.1
8		22.9

(2) Physical widths of scintillators (w) and range of electron radii which can be detected (Δr).

Counter Number	180-deg Spectrometer		Circular Spectrometer	
	w (in.)	Δr	w (in.)	Δr
1	1	0.5	0.94	0.53
2	1	0.5	1.13	0.69
3	1	0.5	1.28	0.86
4	1	0.5	1.41	1.04
5	1	0.5	1.47	1.26
6	1	0.5	1.50	1.51
7			1.47	1.80
8			1.41	2.15

Note: In the circular spectrometer, the widths w were chosen so that $\Delta r/r$ and thus $\Delta k/k$ would remain constant.

(3) Values of magnetic field at which data were taken.

Number	Magnetic field (kgauss)	Number	Magnetic field (kgauss)
1	1.92	9	6.64
2	2.24	10	7.76
3	2.62	11	9.06
4	3.06	12	10.59
5	3.57	13	12.36
6	4.17	14	14.44
7	4.87	15	16.87
8	5.69	16	19.70

Note: Successive field settings were chosen such that $H_{j+1} = 1.168\ H_j$.

(4) Electron energies at maximum field setting.

(H = 19.70 kgauss)

Counter Number	180-deg Spectrometer (MeV)	Circular Spectrometer (MeV)
1	45	84
2	60	109
3	75	136
4	90	166
5	105	200
6	120	239
7		286
8		343

D. Vertical Scattering Correction

The spectrometer efficiency, as derived in Appendix A, does not take into consideration the fact that some of the electron-positron coincidences will be missed owing to the possibility of one or both electrons scattering vertically out of the plane of the scintillators. Horizontal scattering, however, will not reduce the counting rate, since on the average as many electrons will be scattered into a detector as are scattered out. Only the spectrometer resolution is affected by horizontal scattering, and this is discussed in Appendix B.

We refer to Fig. 24 in setting up the problem for calculating the vertical scattering loss. We assume that a gamma ray of energy k enters one side of a converter of thickness t_0 and height h, at a distance x above the center of the converter. At a point t g/cm^2 from the other side of the converter an electron-positron pair is formed.

We now focus our attention on the positron. We assume it to be emitted in the direction of the gamma ray. The average angle of emission is actually of the order of mc^2/E^+, which is small in comparison with the average scattering angle, and therefore can be ignored. The positron continues a distance t through the remainder of the converter and is scattered through a projected angle ϕ. We use the projected angle instead of the space angle in order to include only the vertical component of scattering. The distribution in ϕ depends upon the energy of the positron and the thickness of the converter.

We now ask the question: What is the probability that the positron will enter the scintillator and be detected? More specifically, if the scintillator has a height a, and the positron must travel a distance D^+ to the scintillator (since, it is in a magnetic field, it actually travels along the arc of a circle), what is the probability that the positron will be scattered less than an angle ϕ_1^+ up or ϕ_2^+ down?

We let $P(\phi, t, E)$ represent the probability that the projected scattering angle will be less than ϕ when an electron or positron of total energy E passes through a thickness t g/cm^2 of tantalum. The form of P will be considered later. The probability of the positron being detected is then

$$\frac{1}{2}\left[P(\phi_1^+, t, E^+) + P(\phi_2^+, t, E^+)\right],$$

where

$$\phi_1^+ = \tan^{-1}\left(\frac{\frac{a}{2} + x}{D^+}\right),$$

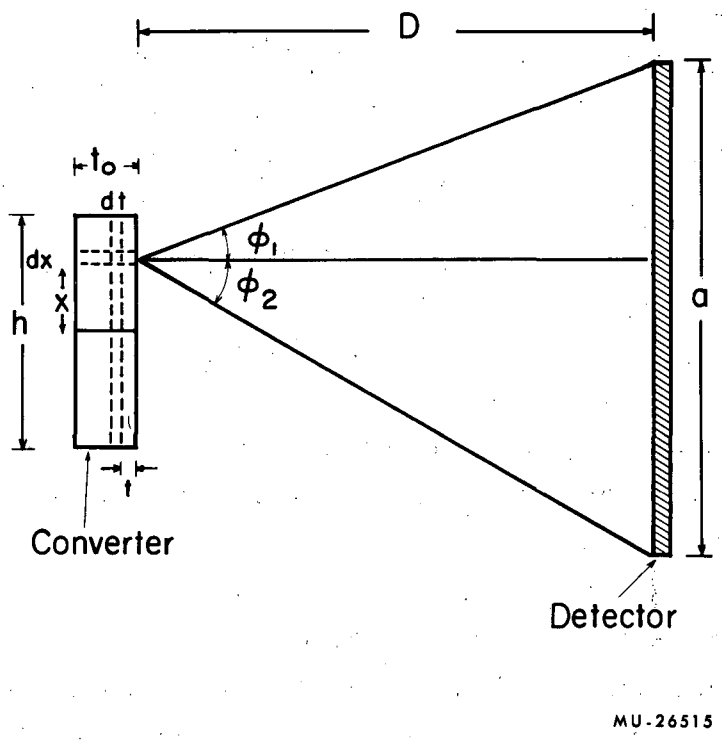

Fig. 24. Diagram to perform the vertical scattering correlation calculation. The distance D is actually along the arc of a circle.

and $$\phi_2^{+} = \tan^{-1}\left(\frac{\frac{a}{2} + x}{D^{+}}\right).$$

Similar expressions can be written down for the electron probability. Since the scattering of the electron is independent of the scattering of the positron, the total probability of both particles entering a scintillator is the product of the individual probabilities.

We may now compute an average probability over the whole converter by performing a double integration: one over the height and one through the thickness of the converter. The integral to be evaluated is

$$P_{av} = \frac{1}{4}\frac{2}{h\,t_0}\int_{x=0}^{h/2} dx \int_{t=0}^{t_0} dt \left[P(\phi_1^{+}, t, E^{+}) + P(\phi_2^{+}, t, E^{+})\right] \times \left[P(\phi_1^{-}, t, E^{-}) + P(\phi_2^{-}, t, E^{-})\right].$$

An underlying assumption in this integral is that equal numbers of pairs are produced over the thickness and height of the converter. This would not hold for thick converters, or for converters partially shadowed by collimation of the gamma rays.

The value of $P(\phi, t, E)$ must be obtained from electron scattering theory. Let us denote the probability of finding an electron of energy E emerging from a thickness t (g/cm^2) of tantalum with a projected angle between α and $\alpha + d\alpha$ as $f(\alpha, t, E)\, d\alpha$. Then

$$P(\phi, t, E) = \int_0^{\phi} f(\alpha, t, E)\, d\alpha.$$

If we do not require a high degree of accuracy, $f(\alpha, t, E)\, d\alpha$ may be approximated by a Gauss error curve:

$$f(\alpha, t, E)\, d\alpha = \frac{1}{\sqrt{2\pi\overline{\alpha^2}}} \exp\left(-\alpha^2/2\overline{\alpha^2}\right) d\alpha,$$

where

$$\overline{\alpha^2} = \frac{14}{E}\sqrt{t'},$$

in which t' = thickness in radiation lengths, and E = electron energy measured in MeV.

For greater accuracy, one must consider deviations from a pure Gaussian, especially for a thin converter, where the number of scattering collisions is small. In our calculation we used the more exact plural scattering theory of Molière. Since the formalism of this theory is somewhat complex, it will not be reproduced here. It is summarized in Bethe and Ashkin,[37] except for some of the projected angle formulas that must be obtained from the original.

The double integral over the converter was evaluated by using a ten-point Simpson's rule approximation. It must be calculated for each spectrometer, for each converter used, and for each combination at each magnetic field. The time required on the IBM 709 was about 20 minutes for one converter.

If the simplified Gaussian form for the scattering angle distribution is used, one can easily show that for a 180-deg spectrometer, the scattering loss is independent of counter combination at a given magnetic field. Using our more exact formulae, it was indeed found that the efficiencies at the same field varied less than 1%. However, this was no longer true for the circular spectrometer, where efficiencies of different counter combinations could vary by as much as 20 or 30% at a given field setting.

E. Pair-Production Cross-Section Formulae

The pair-production cross sections used in the calculations on spectrometer efficiency (see Appendix A) are those given by Bethe and Heitler,[34] as summarized by Bethe and Ashkin[37] and modified by Davies et al.[38] to account for deviations from the Born approximation. The differential cross section for the creation of a positron of total energy between E^+ and $E^+ + dE^+$ and a negative electron E^- by a gamma ray of energy k, denoted by $\underline{\phi}(k, E^+)\, dE^+$ is given by

$$\underline{\phi}(k, E^+)\, dE^+ = \frac{\bar{\underline{\phi}}\, dE^+}{k} \quad G(k, E^+),$$

where

$$\bar{\underline{\phi}} = \frac{Z(Z+\zeta)}{137} \; r_0^2 = Z(Z+\zeta) \times 5.793 \times 10^{-28} \text{ cm}^2,$$

with

$$r_0 = \frac{e^2}{mc^2} = 2.82 \times 10^{-13} \text{ cm}.$$

The ζ is a quantity slightly greater than unity ($\zeta \approx 1.17$ for Ta) which accounts for pair production in the field of electrons, and m is the electron mass.

$G(k, E^+)$ is a slowly-varying function that depends upon the screening effect of the atomic electrons. We define a quanity γ:

$$\gamma = 100 \; \frac{k\, mc^2}{E^+ E^- Z^{1/3}} .$$

For tantalum, with energies measured in MeV, we have

$$\gamma = 12.23 \; \frac{k}{E^+ E^-} .$$

Then $G(k, E^+)$ is defined in two regions:

Region I: $0 < \gamma \leq 2$

$$G(k, E^+) = \frac{1}{k^2} \left\{ (E^{+2} + E^{-2}) \left[\phi_1(\gamma) - \frac{4}{3} \log Z - 4f(Z) \right] + \frac{2}{3} E^+ E^- \left[\phi_2(\gamma) - \frac{4}{3} \log Z - 4f(Z) \right] \right\}$$

$\phi_1(\gamma)$ and $\phi_2(\gamma)$ are functions given graphically in Bethe and Ashkin.[37] In our computer program these were approximated by polynomials:

for $0 < \gamma \leq 1$,

$$\phi_1(\gamma) = 20.76 - 4.00\,\gamma + 0.78\,\gamma^2,$$

and

$$\phi_2(\gamma) = 20.17 - 2.78\,\gamma + 0.12\,\gamma^2;$$

and for $1 < \gamma \leq 2$,

$$\phi_1(\gamma) = \phi_2(\gamma) = 20.68 - 3.63\,\gamma + 0.56\,\gamma^2 .$$

The f(Z) is the correction term to the Born approximation given by Davies et al.[38] For tantalum, f(73) = 0.2756.

Region II: $\gamma > 2$

$$G(k, E^+) = \frac{4}{k^2}(E^{+2} + E^{-2} + \frac{2}{3}\,E^+E^-) \times \left[\log \frac{2\,E^+E^-}{k\,mc^2} - \frac{1}{2} - c(\gamma) - f(Z)\right] .$$

The $C(\gamma)$ is plotted in Bethe and Ashkin.[37] This was approximated in our program by

$$c(\gamma) = \frac{1}{3.18\,\gamma - 1.59} .$$

In our computer calculation of spectrometer efficiency, $G(k, E^+)$ was calculated for each counter combination at each magnetic field, and the result multiplied by the corresponding geometry and scattering loss factors as derived in Appendices A and D.

F. The Kinematics of π^0 Decay

We consider in this Appendix the angular and energy distribution of gamma rays produced by the following process:

$$p + p \rightarrow p + p + \pi^0,$$

$$\pi^0 \rightarrow \gamma + \gamma .$$

We thus have three different frames of reference to consider:

(a) The rest frame of the decaying pion;

(b) The center-of-mass frame of the incident protons; and

(c) The laboratory frame, in which measurements are made.

The simplest of these is the pion rest frame. Each pion decays into two gamma rays of equal energy (67.5 MeV, half the pion rest mass). These gamma rays emerge in opposite directions, and since the pion has no spin and therefore can have no orientation in space, every direction is equally probable.

In the two-proton c.m. system, the final state is a three-body state. Thus the pion can have any energy ranging from zero up to a kinematically determined maximum, which occurs when the pion emerges in one direction and the two protons emerge together in the opposite direction.

The probability that the pion will emerge at a given c.m. angle θ' with respect to the line joining the two incoming protons is given by a certain distribution function determined by the nature of the interaction. Even without knowledge of any of the details of this interaction we can deduce certain properties of this distrubiton function:

First, it must depend only upon the angle θ', and not the azimuthal angle ϕ, so long as both protons are completely unpolarized.

Second and most important, since the two protons are indistinguishable in the c.m. frame, all pion (and therefore gamma-ray) distributions, both angular and energy, must have symmetry about a plane perpendicular to the line joining the incoming protons. Thus, observations (in the c.m. system) at angle θ' must be equivalent to those at $180^\circ - \theta'$. If we expand any angular distribution function in powers of cos θ', even powers only can appear.

In the first part below we derive the differential cross sections and spectra for gamma-ray production in the two-proton center of mass, assuming arbitrary pion distributions. In Part 2 we relate the laboratory and c.m.

gamma ray spectra. In Part 3 we relate the coincidence rate of the spectrometer to the total cross section for pion production.

1. Determination of Gamma-Ray Spectra from π^0 Distributions.

We assume that the neutral pions are produced with velocity $v' = \beta' c$ in the proton-proton c.m. system, with a total cross section σ_{π^0}. (Throughout this Appendix primes refer to quantities in the center-of-mass system.) The restriction that the pions be mono-energetic will be removed later. Let us express the pion angular distribution in terms of Legendre polynomials, such that

$$\frac{d\sigma_{\pi^0}}{d\Omega'} = \sigma_{\pi^0} \sum_n a_n P_n(\cos\theta') .$$

Then it can be shown (see Appendix A, thesis by Robert Squire[39]) that the differential cross section for production of gamma rays in the c.m. system is given by

$$\frac{d^2\sigma_\gamma}{d\Omega' dk'} = \frac{\sigma_{\pi^0}}{\beta'\gamma' k_0} \sum_n a_n P_n(\cos\theta') P_n(z)$$

for k' within the limits $\gamma'(1-\beta') < \frac{k'}{k_0} < \gamma'(1+\beta')$; and

$$\frac{d^2\sigma_\gamma}{d\Omega' dk'} = 0$$

for k' outside these limits.

Here $k_0 = \frac{\mu_{\pi^0}}{2} = 67.5$ MeV, and $z = \cos\alpha$, where α is the angle between the direction of the photon and the direction of the π^0 which produced it. From relativity theory,

$$k' = \frac{k_0}{\gamma'(1-\beta'\cos\alpha)}$$

and therefore

$$z = \cos\alpha = \frac{1}{\beta'}\left(1 - \frac{k_0}{\gamma' k'}\right) .$$

We now consider four special cases:

Case 1. Neutral pions produced isotropically.

Here we have

$$\frac{d\sigma_{\pi^0}}{d\Omega'} = \frac{\sigma_{\pi^0}}{4\pi} \; ; \; a_0 = \frac{1}{4\pi}$$

then

$$\frac{d^2\sigma_\gamma}{d\Omega' dk'} = \frac{\sigma_{\pi^0}}{4\pi\beta'\gamma' k_0} ,$$

for $\gamma'(1-\beta') < \frac{k'}{k_0} < \gamma'(1+\beta')$; and

$$\frac{d^2\sigma_\gamma}{d\Omega' dk'} = 0, \text{ otherwise.}$$

If the pions are not mono-energetic, but are distributed so that $h_0(p')dp'$ represents the number of pions with momentum between p' and $p'+dp'$, normalized so that $\int h_0(p')dp' = 1$, then

$$\frac{d^2\sigma_\gamma}{d\Omega' dk'} = \frac{\sigma_{\pi^0}}{4\pi k_0} \int_{p' = \frac{1}{2\lambda}|\lambda^2 - 1|}^{p'_{max}} \frac{h_0(p')}{p'} dp' .$$

Here $\lambda = \frac{k'}{k_0}$ and the momentum p' is measured in units of $\mu_{\pi^0}c$. In these units, $p' = \beta'\gamma'$.

Case 2. Pions produced with a pure $\cos^2\theta'$ distribution.

Here we have

$$\frac{d\sigma_{\pi^0}}{d\Omega'} = \frac{3\sigma_{\pi^0}\cos^2\theta'}{4\pi} ; \quad a_0 = \frac{1}{4\pi} , \quad a_2 = \frac{2}{4\pi} ;$$

then

$$\frac{d^2\sigma_\gamma}{d\Omega' dk'} = \frac{3\sigma_{\pi^0}}{8\pi\beta'\gamma' k_0} (M + N z^2) ,$$

where

$$M = 1 - \cos^2\theta' ,$$

$$N = 3\cos^2\theta' - 1 .$$

If the pions have a momentum distribution $h_2(p)$, then

$$\frac{d^2\sigma_\gamma}{d\Omega' dk'} = \frac{3\sigma_{\pi^0}}{8\pi k_0} \int_{p' = \frac{1}{2\lambda}|\lambda^2 - 1|}^{p'_{max}} \frac{h_2(p')}{p'} (M + N z^2) dp' .$$

Note that at the "isotropic angle", for which $\cos^2\theta' = 1/3$, this reduces to the same form as that for isotropic production, including the normalization factor.

Case 3. Pions produced with pure $\cos^4\theta'$ distribution.

Here we have

$$\frac{d\sigma_{\pi^0}}{d\Omega'} = \frac{5\,\sigma_{\pi^0}\cos^4\theta'}{4\pi} \quad ;$$

$$a_0 = \frac{1}{4\pi}\,,\quad a_2 = \frac{5}{7\pi}\,,\quad a_4 = \frac{2}{7\pi}$$

and if the pions have a momentum distribution $h_4(p')$, then

$$\frac{d^2\sigma_\gamma}{d\Omega'\,dk'} = \frac{5\,\sigma_{\pi^0}}{32\,\pi\,k_0} \int_{p'=\frac{1}{2\lambda}\left|\lambda^2-1\right|}^{p'_{max}} \frac{h_4(p')}{p'}\,(3M^2 - 6Rz^2 + Sz^4)\,dp' \,.$$

where

$$M = 1 - \cos^2\theta',$$
$$R = (1 - \cos^2\theta')(1 - 5\cos^2\theta'),$$
$$S = 35\cos^4\theta' - 30\cos^2\theta' + 3\,.$$

Case 4: Combination isotropic plus $\cos^2\theta'$, with arbitrary parameter b.

Here we have

$$\frac{d^2\sigma_{\pi^0}}{d\Omega'} = \frac{3\sigma_{\pi^0}}{4\pi}\left(\frac{\frac{1}{3} + b\cos^2\theta'}{1+b}\right) \quad ;$$

then

$$\frac{d^2\sigma_\gamma}{d\Omega'\,dk'} = \frac{\sigma_{\pi^0}}{8\pi\,k_0(1+b)} \times \int_{p'=\frac{1}{2\lambda}\left|\lambda^2-1\right|}^{p'_{max}} \frac{2h_0(p') + 3b\,h_2(p')(M + N z^2)}{p'}\,dp' \,.$$

In Fig. 25 we show the resulting gamma-ray spectra at angles of 0, 55, and 90 deg, for isotropic, $\cos^2\theta'$, and $\cos^4\theta'$ pion distributions, where we assume a momentum distribution proportional to the three-body phase space factor at 735 MeV:

$$h(p) \propto p^2 \left(E - \sqrt{p^2+1} - \frac{p^2}{4M} \right)^{1/2},$$

where E is the available c. m. kinetic energy before pion production, and M is the proton rest mass. All quantities are measured in units of pion rest masses. The energy scales are logarithmic in order to illustrate the symmetry properties. The spectra are normalized to $\sigma_{\pi^0} = 1$.

2. Transformation of Gamma Ray Spectra

Let us assume that the differential cross section for producing gamma rays in the c. m. system is given by $\frac{d^2\sigma_\gamma}{d\Omega' dk'}$. We wish to calculate the equivalent quantity in a frame such as the laboratory frame moving with velocity β with respect to the center of mass. From basic principles of relativity, it can be shown that the gamma-ray transformation equations for solid angle and energy are:

$$\frac{d\Omega_{lab}}{d\Omega'} = \gamma^2 (1 - \beta \cos\theta_{lab})^2 = \frac{1}{\gamma^2(1+\beta\cos\theta')^2},$$

and

$$k_{lab} = \frac{k'}{\gamma(1-\beta\cos\theta_{lab})} = k'\gamma(1+\beta\cos\theta').$$

Also we have

$$\cos\theta_{lab} = \frac{\cos\theta'+\beta}{1+\beta\cos\theta'}.$$

We use these formulae, then, to determine that

$$\left(\frac{d^2\sigma_\gamma}{d\Omega_{lab}dk_{lab}}\right)_{\theta_{lab},k_{lab}} = \gamma(1+\beta\cos\theta')\left(\frac{d^2\sigma_\gamma}{d\Omega' dk'}\right)_{\theta',k'},$$

and

$$\left(\frac{d^2\sigma_\gamma}{d\Omega' dk'}\right)_{\theta',k'} = \gamma(1-\beta\cos\theta_{lab})\left(\frac{d^2\sigma_\gamma}{d\Omega_{lab}dk_{lab}}\right)_{\theta_{lab},k_{lab}},$$

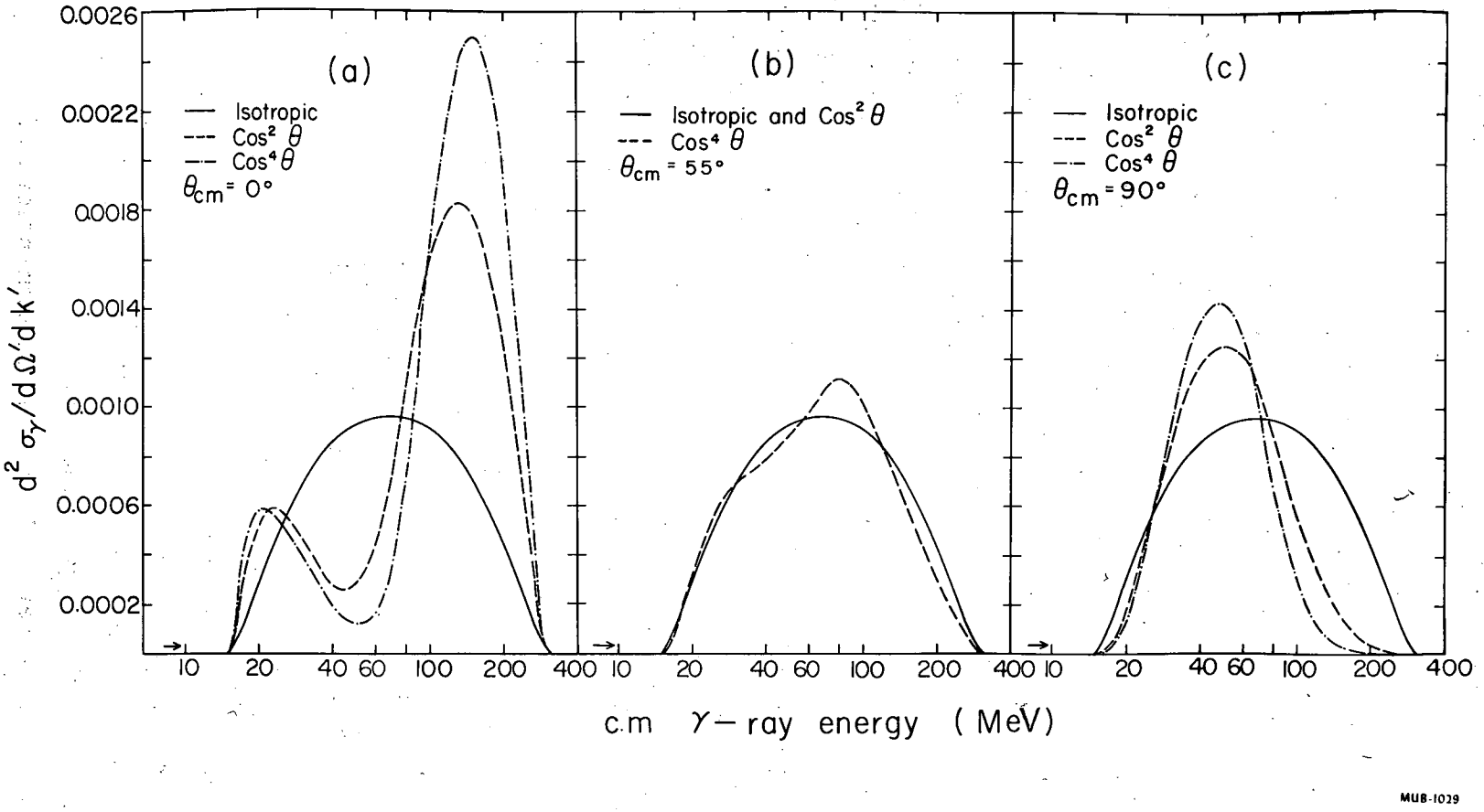

Fig. 25. Theoretical gamma-ray spectra at three c.m. angles from the decay of pions with various angular distributions. Note the degeneracy at the isotropic angle (55 deg).

where θ_{lab}, θ', k_{lab}, and k' are related as above. To transform a laboratory spectrum at a given laboratory angle to an equivalent c.m. spectrum at a corresponding c.m. angle, one needs only to multiply both the energy and value of each experimental point by the factor $\gamma(1-\beta \cos \theta_{lab})$. If the spectrum has been plotted on a log-log scale, this is equivalent to moving the entire spectrum along a 45-deg line.

Because the transformations for gamma-ray spectra are so straightforward, our procedure has been to transform all spectra measured in the laboratory to the equivalent spectra in the center of mass immediately. All further analysis is performed in the center of mass, with no further reference to the laboratory spectra.

3. Determination of Total Cross Section

We may now proceed to link together the results of Sections 1 and 2 above, and in addition the results of Appendices A and E, to determine the total cross section for pion production σ_{π^0}. We assume that N protons pass through a hydrogen target of thickness t_H g/cm^2. At an angle θ_{lab} and a distance R cm from the target, we place a converter made of material of atomic number Z_c and atomic weight A_c, of area ℓ^2 and thickness t_c g/cm^2. A pair of counters are located in a magnetic field H so that they will observe positrons and electrons whose average radius of curvature is r^+ and r^-, and average energy is E^+ and E^-. Then the number of coincidences observed, C, is given by

$$C = N \frac{N_0 t_H}{A_H} \sigma_{\pi^0} \frac{f(k',\theta')}{1-\beta \cos \theta_{lab}} \frac{\ell^2}{R^2} \frac{N_0 t_c}{A_c}$$

$$\times \left[\overline{\underline{\Phi}}\, G(k_{lab}, E^+)\right] \left[\frac{aH \Delta r^+ \Delta r^-}{r^+ + r^-}\right],$$

where

N_0 = Avogadro's number,

A_H = atomic weight of hydrogen = 1.008,

β = velocity of the c.m. system,

$\overline{\underline{\Phi}}$ and $G(k_{lab}, E^+)$ are defined in Appendix E,

Δr^+ and Δr^- are defined in Appendices A and C,

a is a constant chosen so that a H Δr^+ has the dimensions of energy,

$f(k', \theta')$ is the function derived in Part 1 above, normalized so that

$$\frac{d^2\sigma_\gamma}{d\Omega' dk'} = \sigma_{\pi^0} f(k', \theta') .$$

This function, of course, depends upon the energy and angular distributions of the pion.

Note that the expression for C has not been corrected for vertical scattering losses or for the effect of radiation straggling.

ACKNOWLEDGMENTS

I wish to thank Professor Burton J. Moyer for originally suggesting this experiment and for his continued interest and guidance during the course of my research studies. Throughout many years he has maintained a strong interest in the characteristics of the neutral pion and the methods of pair spectrometry used to study it.

Dr. Robert Cence has guided this experiment since its inception and has been a full partner in all phases of planning, execution and analysis. Mr. Don Lind has also been a close associate, especially in the design of equipment and the development of techniques of data analysis. Mr. Paul McManigal wrote the earliest version of the data analysis program, and he and Mr. Donald Hagge were of invaluable assistance during our cyclotron runs.

Mr. James Vale and his staff operated the cyclotron, and Mr. Robert Walton was responsible for setup. Miss Miriam Machlis did the typing and was helpful in setting up the paper in its final form. To all these people I wish to extend my sincere appreciation.

This work was done under the auspices of the United States Atomic Energy Commission.

REFERENCES

1. A. H. Rosenfeld, Phys. Rev. 96, 139 (1954).
2. M. Gell-Mann and K. H. Watson, Ann. Rev. Nucl. Sci. 4, 219 (1954).
3. S. J. Lindenbaum and R. M. Sternheimer, Phys. Rev. 105, 1874 (1957).
4. R. M. Sternheimer and S. J. Lindenbaum, Phys. Rev. 123, 333 (1961).
5. E. Fermi, Progr. Theoret. Phys. (Kyoto) 5, 570 (1950); Phys. Rev. 92, 452 (1953).
6. S. Mandelstam, Proc. Roy. Soc. (London), Ser. A, 244, 491 (1958).
7. F. Bonsignori and F. Selleri, Nuovo cimento 15, 465 (1960).
8. F. Selleri, Phys. Rev. Letters 6, 62 (1961).
9. J. Iizuka and A. Klein, Phys. Rev. 123, 669 (1961).
10. A. P. Batson, B. B. Culwick, J. G. Hill, and L. Riddiford, Proc. Roy. Soc. (London), Ser. A 251, 218 (1959).
11. R. Bjorklund, W. E. Crandall, B. J. Moyer, and H. F. York, Phys. Rev. 77, 213 (1950).
12. J. Steinberger, W. K. H. Panofsky, and J. Steller, Phys. Rev. 78, 802 (1950).
13. R. W. Hales, R. H. Hildebrand, N. Knable, and B. J. Moyer, Phys. Rev. 85, 373 (1952); R. W. Hales and B. J. Moyer, Phys. Rev. 89, 1047 (1953).
14. J. W. Mather and E. A. Martinelli, Phys. Rev. 92, 780 (1953).
15. B. J. Moyer and K. R. Squire, Phys. Rev. 107, 283 (1957).
16. J. Marshall, L. Marshall, V. A. Nedzel, and S. D. Warshaw, Phys. Rev. 88, 632 (1952).
17. R. A. Stallwood, R. B. Sutton, T. H. Fields, J. G. Fox, and J. A. Kane, Phys. Rev. 109, 1716 (1958); R. A. Stallwood (Ph. D. Thesis) Carnegie Institute of Technology Report NYO-7108, March 1956 (unpublished).
18. C. York, R. March, W. Kernan, and J. Fischer, Phys. Rev. 113, 1339 (1959).
19. W. E. Crandall and B. J. Moyer, Phys. Rev. 92, 749 (1953); W. E. Crandall (Ph. D. Thesis), Lawrence Radiation Laboratory Report UCRL-1637, 1952 (unpublished).
20. A. A. Tiapkin, M. S. Kozadaev, and Iu. D. Prokoshkin, Dokl. Akad. Nauk SSSR 100, 689 (1955).

21. L. M. Soroko, Soviet Phys. JETP (English Transl.) 3,184 (1956).
22. Iu. D. Prokoshkin and A. A. Tiapkin, Soviet Phys. JETP (English Transl.) 5, 618 (1957).
23. A. F. Dunaitsev and Iu. D. Prokoshkin, Soviet Phys. JETP (English Transl.) 9, 1179 (1959).
24. I. S. Hughes, P. V. March, H. Muirhead, and W. O. Lock, Phil. Mag., Ser. 8 2, 215 (1957).
25. Iu. D. Baiukov and A. A. Tiapkin, Soviet Phys. JETP (English Transl.) 5, 779 (1957).
26. G. B. Chadwick, G. B. Collins, C. E. Swartz, A. Roberts, S. Benedetti, N. C. Hein, and P. J. Duke, Phys. Rev. Letters 4, 611 (1960).
27. N. C. Hein (Thesis), Carnegie Institute of Technology Report NYO-9285, May 1961 (unpublished); G. B. Collins, Bull. Am. Phys. Soc., Ser. 2, 7, 68 (1962).
28. Iu. D. Baiukov, M. S. Kozodaev, and A. A. Tiapkin, Soviet Phys. JETP (English Transl.) 5, 552 (1957).
29. A. A. Tiapkin, Soviet Phys. JETP (English Transl.) 3, 979 (1956).
30. Iu. D. Prokoshkin, Soviet Phys. JETP (English Transl.) 4, 618 (1956).
31. S. Von Friesen and W. Barkas, Structure of the External Beam of the 184-inch Cyclotron, Lawrence Radiation Laboratory Report UCID-613, Jan. 1959 (unpublished).
32. R. Larsen, Experiments on Neutron-Proton Scattering and Determination of the Pion-Nucleon Coupling Constant (Thesis), Lawrence Radiation Laboratory Report UCRL-9292, July 1960 (unpublished).
33. W. Wenzel, Millimicrosecond Coincidence Circuit for High-Speed Counting, Lawrence Radiation Laboratory Report UCRL-8000, Oct. 1957 (unpublished).
34. H. A. Bethe and W. Heitler, Proc. Roy. Soc. (London), Ser. A, 146, 83 (1934).
35. James Ryan, Lawrence Radiation Laboratory, Berkeley (private communication).
36. G. Molière, Z. Naturforsch. 3a, 78 (1948).
37. H. A. Bethe and J. Ashkin, Passage of Radiations through Matter, in Experimental Nuclear Physics, Vol. I. edited by E. Segrè (John Wiley and Sons, Inc., New York, 1953).
38. H. Davies, H. A. Bethe, and L. C. Maximon, Phys. Rev. 93, 788 (1954).

39. R. Squire, Characteristics of the Production of Neutral Mesons near Threshold in p-p Collisions (Thesis), Lawrence Radiation Laboratory Report UCRL-3137, Sept. 1955 (unpublished).